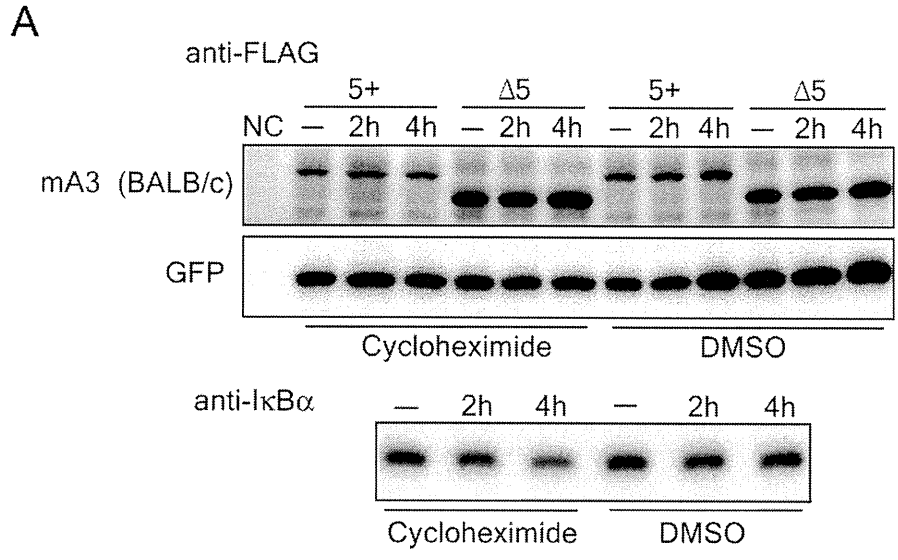
A
anti-FLAG
5+
Δ5
5+
Δ5
NC — 2h 4h — 2h 4h — 2h 4h — 2h 4h
mA3 (BALB/c)
GFP
Cycloheximide
DMSO
anti-IκBα
— 2h 4h — 2h 4h
Cycloheximide
DMSO

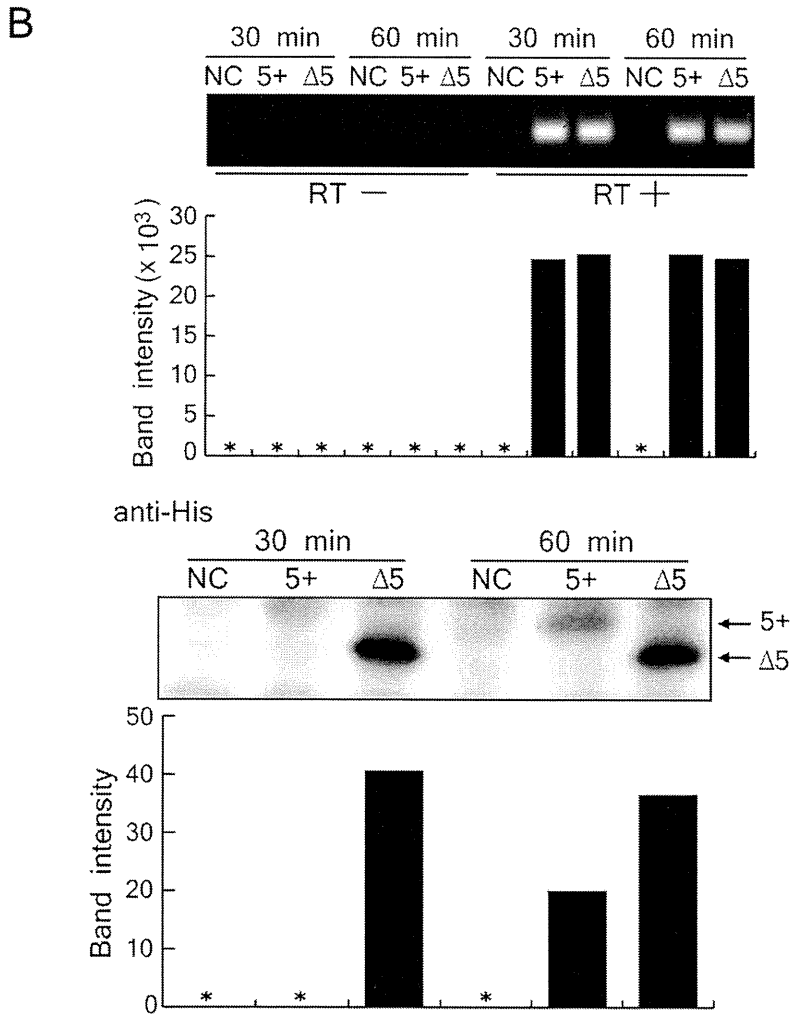
B
30 min
60 min
30 min
60 min
NC 5+ Δ5 NC 5+ Δ5 NC 5+ Δ5 NC 5+ Δ5
RT —
RT +
Band intensity (x 10³)
30
25
20
15
10
5
0
anti-His
30 min
60 min
NC 5+ Δ5 NC 5+ Δ5
5+
Δ5
Band intensity
50
40
30
20
10
0

Figure 3. The presence of exon 5 does not affect protein degradation but exhibits a profound impact on mA3 protein synthesis. (A) 293T cells were transfected with pFLAG-CMV2-*mA3*^{d} or pFLAG-CMV2-*mA3*$^{d}\Delta5$ along with pFLAG-CMV2-GFP, which expresses green fluorescent protein (GFP) as a loading control. The cells were treated with cycloheximide for the indicated duration to stop protein synthesis and then harvested. DMSO was used as a solvent control. The FLAG-tagged mA3 and GFP were detected with the anti-FLAG antibody in immunoblotting. Endogenous IκBα expression was used as a positive control to confirm the effect of cycloheximide. (B) *In vitro* transcription and translation assays. DNA templates containing the entire coding region of the BALB/c full-length or Δ5 mA3 cDNA with the T7 promoter and His-tag sequence were subjected to an *in vitro* transcription/translation reaction by incubating for 30 or 60 min. The levels of mA3 protein synthesis and mRNA expression were evaluated by immunoblotting using the anti-His antibody and RT-PCR using the primer set a-b, respectively. Intensities of protein bands on the immunoblot membrane and DNA bands after the RT-PCR reaction and electrophoresis were measured by densitometry and are shown below each corresponding band. *, signals below detection limits.
doi:10.1371/journal.ppat.1002478.g003

while transfection with the corresponding BALB C741T and the wild-type BALB exon 4–7 clearly resulted in the generation of the 5+ mRNA. These results indicate that polymorphisms other than those in intron 4 might play more important roles in determining exon 5 inclusion into mA3 messages.

A region around the exon 5/intron 5 boundary contains a major determinant for exon 5 inclusion

As abundant expression of the exon 5-containing message was found with the BALB C741T but not with the B6 +TCCT construct, we were prompted to examine other polymorphisms downstream of intron 4 that might be involved in the splicing of exon 5. To explore other possible sequence variations required for exon 5 inclusion, we focused on intron 5, since this region contains numerous polymorphisms between reported genomic sequences of different mouse strains (Figure 5A). Splicing assay vectors harboring the genomic DNA fragment containing exons 5 and 6 along with the entire intron 5, from either the B6 or the BALB/c allele, were constructed and designated B6 exon 5–6 or BALB exon 5–6 (Figure 5B). BALB/3T3 cells transfected with the BALB exon 5–6 plasmid generated the properly spliced product of the expected size (Figure 5C), indicating that the splice donor site

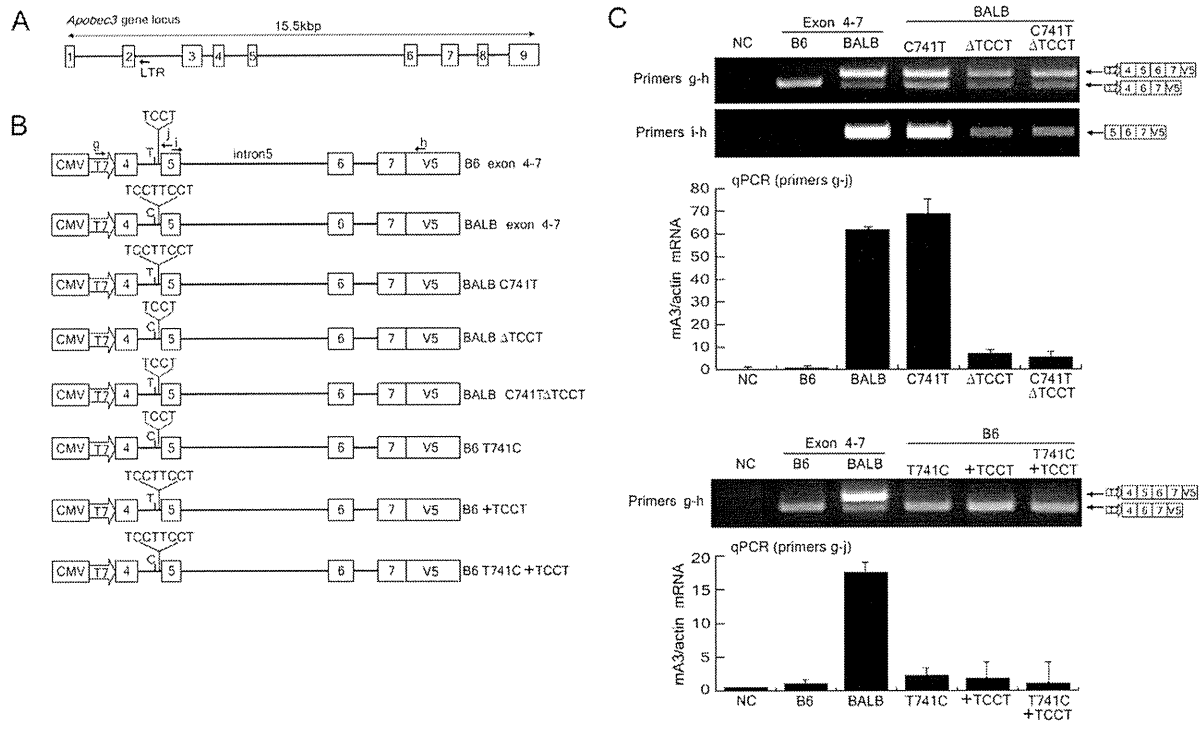

Figure 4. The impact of TCCT repeat numbers on exon 5 inclusion in mA3 mRNA splicing. (A) Schematic representation of the genomic DNA structure of the *Apobec3* gene locus. Boxes indicate exons. LTR, the endogenous retroviral LTR inserted into intron 2 in some strains of mice [37]. (B) Insert structures of the plasmids used for the splicing assays. BALB/c exon 4–7 and BALB/c ΔTCCT plasmids harbored the same DNA fragment amplified from BALB/c genomic DNA encompassing exons 4 and 7, except that the BALB/c ΔTCCT contains only a single TCCT quadruplet. B6 exon 4–7 plasmid harbored the B6 genomic DNA fragment encompassing exons 4 and 7. C741T and T741C indicate a C to T or reciprocal nucleotide substitution, respectively, within intron 4 at 741-bp downstream from the first nucleotide of exon 4 on the backbone of the BALB/c or B6 exon 4–7 insert. An additional repeat of the TCCT quadruplet was added to the B6 exon 4–6 construct to generate B6 +TCCT. The positions of primers g, h, i, and j used for RT-PCR assays are indicated with the arrows. (C) The plasmid harboring each insert depicted in (B) was transfected into BALB/3T3 cells, total RNA was extracted, and RT-PCR reactions were performed with primer pairs g–h and i–h. A portion of the transfected cells were utilized for luciferase assays to compare transfection efficiencies among the samples. Comparable levels of luciferase activities were observed in all samples in each experiment (data not shown). The predicted splicing products are schematically indicated on the right side of the panel. Quantitative real-time PCR assays were performed with primers g and j, and data are shown here by averages of three reaction wells and SD.
doi:10.1371/journal.ppat.1002478.g004

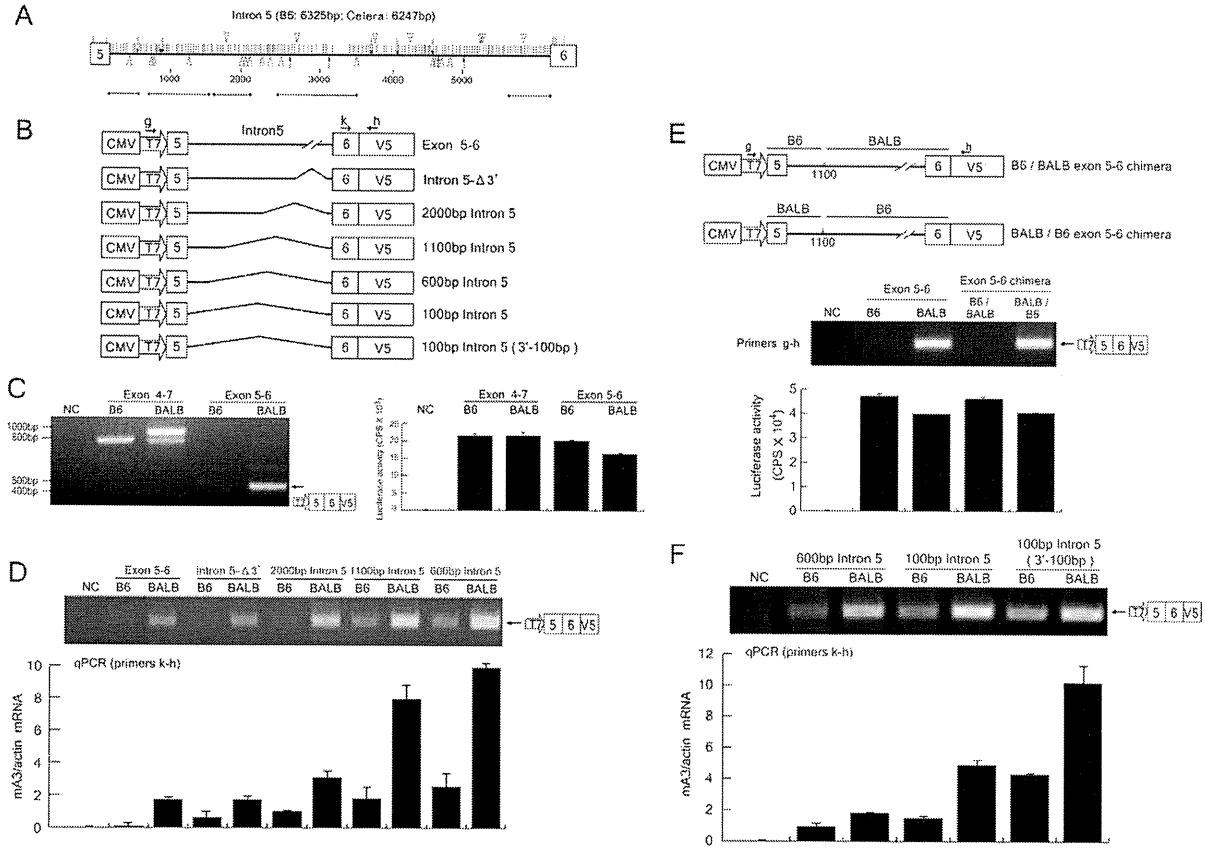

Figure 5. The effect of exon 5 and its downstream sequences on mA3 intron 5 splicing. (A) Distributions of sequence polymorphisms in the intron 5 of the *Apobec3* gene locus between the B6 allele [NT_039621] and the Celera database sequence of mixed mouse DNA [NW_001030577.1]. Shorter horizontal lines below the thick one representing intron 5 indicate regions of sequenced BALB/c genome [DDBJ accession No. AB646261-AB646265], which show nucleotide sequences identical to corresponding Celera database sequences. Spans of the analyzed regions are 1–620, 661–1597, 1643–2058, 2759–3443, and 5558–6247 in base numbers starting from the first nucleotide of intron 5. SNP are shown with vertical lines, single-base indels with arrows, and deletions of ≥2 bases with triangles. Indels and deletions above the thick horizontal line that represents intron 5 are deletions in the B6 allele relative to the Celera sequence, while those underneath the horizontal line are deletions in the Celera sequence relative to the B6 allele sequence. (B) Plasmid constructions for the splicing assays. The exon 5–6 plasmids harbored either the B6 or BALB/c genomic fragment encompassing exons 5 and 6, including the entire intron 5 of the corresponding allele. Each of the remaining plasmids possessed a sequentially reduced length of the intron 5 as indicated. The precise size of each PCR-generated 5′ fragment included was as follows: 3177bp and 3185bp for B6 and BALB/c intron 5-Δ3′; 2106bp and 2086bp for B6 and BALB/c 200bp intron 5; 1120bp and 1110bp for B6 and BALB/c 1100bp intron 5; and 634bp and 620bp for B6 and BALB/c 600bp intron 5, respectively. The primers g–h are the same as shown in Figure 4. (C) RT-PCR detection of spliced messages expressed from the B6 and BALB/c exon 5–6 plasmids along with those from the exon 4–7 plasmids as controls. Primers g and h were used. A lack of expression of the spliced message in cells transfected with the B6 exon 5–6 plasmid was evident. (D and F) Splicing assays using intron 5 deletion plasmids. The intron 5 fragment included in each plasmid is shown in (B). RT-PCR assays were performed with primers g and h. A portion of the transfected cells were utilized for luciferase assays to compare transfection efficiencies among the samples as shown in (C). Comparable levels of luciferase activities were observed in all samples in each experiment (data not shown). Quantitative real-time PCR data show averages of three reaction wells and SD. (E) Reciprocal chimeras were produced between B6 and BALB/c exon 5–6 by exchanging the cloned genomic DNA fragment at position 1100 within intron 5. The exact location of the above position 1100 for B6 and BALB/c intron 5 is described in the legend for (B). RT-PCR detection of spliced messages was performed with primers g and h. A portion of the transfected cells were utilized for luciferase assays to compare transfection efficiencies.
doi:10.1371/journal.ppat.1002478.g005

downstream of exon 5 and the acceptor site upstream of exon 6 in the BALB/c allele are both functional. In contrast, no spliced product was detectable in cells transfected with the B6 exon 5–6 plasmid despite a higher transfection efficiency. These results indicate that the B6 allele may not carry a functional splice donor site at the exon 5/intron 5 boundary, as the splice acceptor site upstream of exon 6 seems intact and thus can generate a message corresponding to the mA3 Δ5 when exon 4 and intron 4 are included (Figures 4 and 5C).

To narrow down the region affecting the intron 5 splicing, serial deletion constructs were produced and subjected to the splicing assay (Figure 5B). The intron 5-Δ3′ is a deletion construct which lacks the 3′ half of intron 5 but retains the 261-bp sequence adjacent to exon 6 to include the putative acceptor site. The cells transfected with the BALB intron 5-Δ3′ plasmid produced the spliced message as efficiently as those transfected with the parental BALB exon 5–6 construct; however, the B6 intron 5-Δ3′ plasmid generated a barely detectable band representing spliced message (Figure 5D). Quantitative real-time PCR assays revealed markedly lower levels of properly spliced message generated from the B6 intron 5-Δ3′ plasmid compared to that generated from the BALB/c counterpart. These data show that the 5′ half of intron 5 is

responsible for the observed differences in splice site functions between the B6 and BALB/c alleles. Thus, further deletions progressively closer to exon 5 were introduced into the intron 5 fragment. As expected, the shorter the included intron 5 fragment, the more abundant the spliced product generated was, regardless of the expressed *Apobec3* alleles, indicating that the intron length of the primary transcript influences the splicing efficiency (Figure 5D). Nevertheless, the spliced product was generated much more efficiently from the BALB/c allele than from the B6 allele with all examined construct pairs, despite comparable levels of transfection efficiency, indicating that each shorter intron fragment still retained the polymorphism responsible for the inefficient splicing of the B6 mRNA.

To exclude the possibility that the 3′ region of intron 5 and/or exon 6 from the B6 allele might harbor inhibitory sequences that interfere with splicing, we constructed chimeras between the BALB and B6 exon 5–6 plasmids by exchanging the corresponding genomic DNA fragments at approximately position 1100 within intron 5 (Figure 5E). BALB/B6 chimera harboring the 5′ donor site sequence from the BALB/c allele and 3′ acceptor site from the B6 allele generated properly spliced mRNA as efficiently as the BALB exon 5–6 plasmid did, while the reciprocal construct harboring the B6 donor and BALB/c acceptor sequences did not (Figure 5E), indicating that there are no inhibitory elements in the fragment harboring the 3′ intron 5 and exon 6 from the B6 allele. Thus, we continued to narrow down the sequence affecting the intron 5 splicing toward the 5′ end of the genomic constructs.

Even the shortest construct pair, B6 100bp intron 5 and BALB 100bp intron 5, which harbor the 5′ intron 5 fragment a mere 100-bp from the exon 5 boundary, still exhibited a readily discernible difference in the amounts of the spliced messages, and this was also true for another pair of deletion constructs that harbor a 100-bp acceptor region fragment of 3′ intron 5 (Figure 5F). These results clearly indicate that the region including exon 5 and the 5′ 100-bp of intron 5 carries the primary determinants responsible for the different efficiencies in splicing of intron 5 shown by the B6 and BALB/c alleles.

A single nucleotide polymorphism within exon 5 is primarily responsible for exon 5 inclusion

Within the above narrowed-down region of exon 5 and the 5′ 100 bp of intron 5, there are only 4 SNPs between the B6 and BALB/c alleles, as previously described [38]: the T/C SNP at 14-bp downstream from the first nucleotide of exon 5, G/C at 88-bp downstream from the same first nucleotide, G/C at 153-bp downstream within intron 5, and A/C at 163-bp downstream within intron 5 (Figure 6A). We therefore produced a series of point mutants based on the B6 intron 5–100 (3′-100bp) and BALB/c intron 5–100 (3′-100bp) constructs to precisely identify the critical SNP responsible for the functionalities of the splice donor site. In the first set of experiments, shown in Figure 6B, each indicated nucleotide within the BALB/c genomic sequence was substituted with the corresponding nucleotide found in the B6 allele. The substitution of the C at position 14 to the B6-type T slightly reduced the amount of the spliced message; more importantly, however, the similar substitution of C at position 88 to the B6-type G totally abrogated the intron 5 splicing. Simultaneous substitutions of C to G at position 153 and G to A at 163 did not affect the generation of the spliced message. Transfection efficiencies were essentially equivalent for all samples and even higher than those for the C88G construct as confirmed by cotransfecting the luciferase expression plasmid (data not shown). These results indicate that the G/C SNP at position 88 in exon 5 is most critical for the splice donor function.

In a reciprocal set of experiments, we attempted to alter splicing of the transcript of the B6 allele by replacing the polymorphic nucleotides with the BALB/c-types (Figure 6C). When all 4 SNPs in the B6 intron 5–100 fragment were replaced with those corresponding to the BALB/c allele, abundant generation of the spliced message was observed (Figure 6C). A combined substitution of T to C and G to C at positions 14 and 88, respectively, also resulted in efficient splicing of intron 5, and a single substitution of T to C at position 14 alone slightly increased the generation of the spliced message from the plasmid harboring the truncated intron. Importantly, a single substitution of G to C at position 88 resulted in as abundant expression of the spliced message as that observed with the BALB/c allele. Thus, these results collectively indicate that the G at position 88 is critical for the exclusion of exon 5, although the C at position 14 may also play a minor role in the inclusion of this exon.

Site-directed mutagenesis of the plasmids harboring the entire intron 5

To determine the association of the above 4 SNPs with splicing efficiency under more physiological conditions, we further introduced point mutations into the B6 exon 5–6 plasmid harboring the entire intron 5 of 6kb in length, and the resultant plasmids were subjected to the splicing assays (Figure 7A). In contrast to the result with the B6 100bp intron 5 T14C mutant (Figure 6C), we could not detect the generation of spliced mRNA after transfection of the B6 exon 5–6 T14C mutant (Figure 7B). However, the single substitution at position 88 from the B6-type G to BALB/c-type C led to readily detectable production of the spliced mRNA, despite the general inefficiency in splicing of the full-length intron 5 depicted in Figure 5. Quantitative real-time PCR assays revealed levels of expression of the exon 5-containing spliced message from the B6 exon 5–6 G88C mutant that were about 70% of those expressed from the BALB exon 5–6 plasmid. Single nucleotide substitutions at two other positions did not result in a detectable generation of the spliced mRNA from the B6 allele (Figure 7B). Combined mutations at positions 14 and 88 within exon 5 on the B6 exon 5–6 construct (B6 exon 5–6 T14C G88C) and further addition of the nucleotide replacements at positions 153 and 163 also resulted in detectable generation of the spliced message, but did not noticeably enhance the splicing over what resulted from the G88C substitution alone (Figure 7C).

Combined effects of the intron 4 TCCT repeat number and exon 5 G/C SNP on exon 5 inclusion into mA3 mRNA

To further compare the effects of the TCCT repeat number and exon 5 G/C SNP at position 88, we constructed B6 and BALB exon 4–7 plasmids that harbored reciprocal substitutions at these two polymorphic sites (Figure 8). Introduction of an additional copy of TCCT into the B6 exon 4–7 construct did not result in the generation of 5+ message, while the combination of the additional TCCT and G88C substitution resulted in the generation of exon 5-containing message at levels comparable to those expressed from the BALB exon 4–7 plasmid. On the other hand, a deletion of a TCCT copy from the BALB exon 4–7 construct resulted in much reduced expression of the 5+ message, and the combination of ΔTCCT and C88G substitution totally abrogated the generation of exon 5-containing message. Thus, these results clearly demonstrate that the most critical polymorphism for exon 5 inclusion into the mA3 mRNA is the G/C SNP at position 88 within exon 5, but for the full-level expression of the 5+ mRNA as observed in BALB/c mice the intron 4 TCCT repeat is also required.

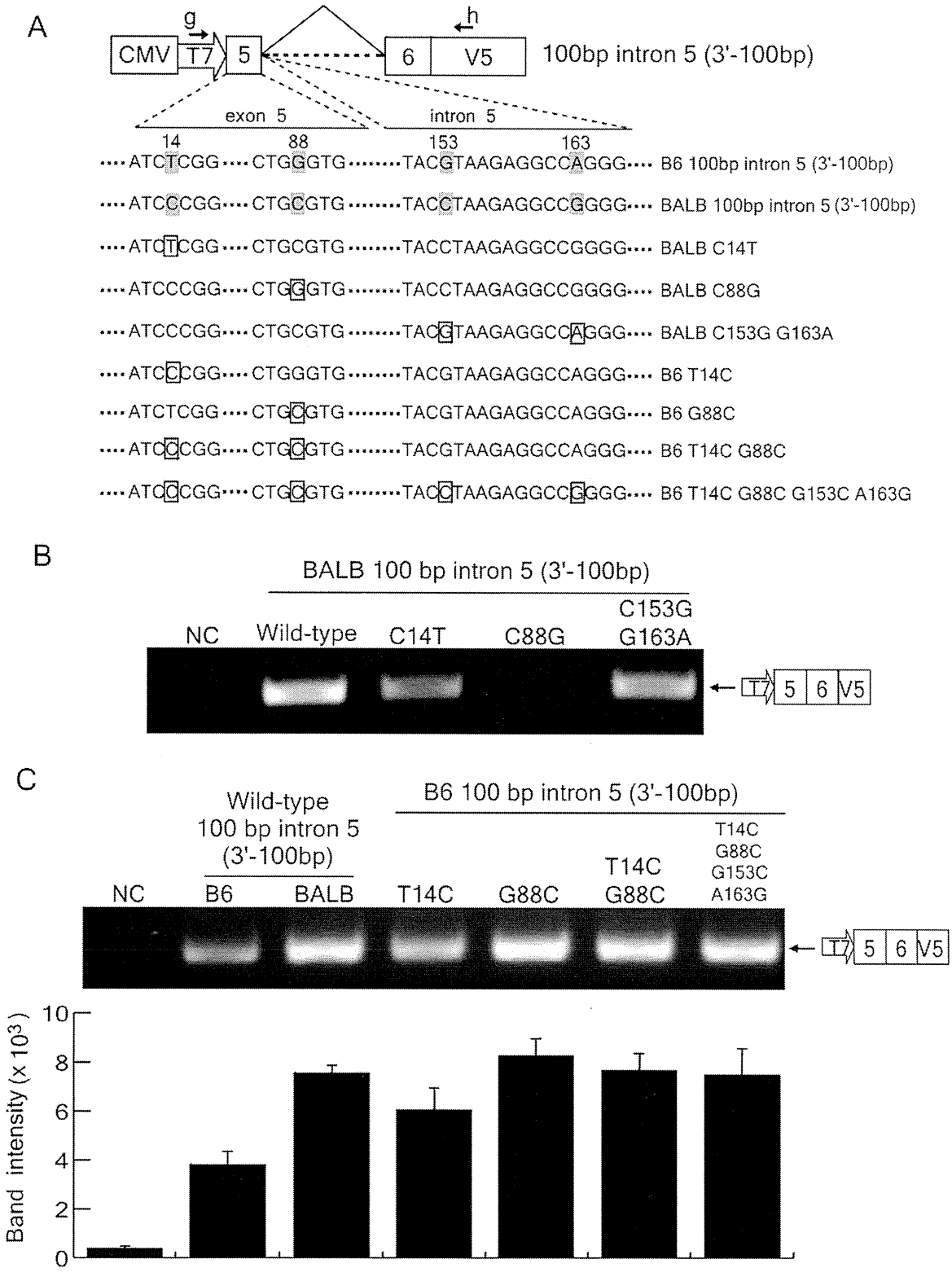

Figure 6. Identification of critical residues for exon 5 inclusion into mA3 mRNA. (A) Polymorphic nucleotides indicated with the shades were exchanged at the boxed sites between the B6 and BALB/c alleles. The numbers 14, 88, 153, and 163 above the shown nucleotide sequence are base numbers from the first nucleotide of exon 5. (B and C) The results of splicing assays performed with the plasmids depicted in (A). The predicted splicing product is shown on the right side of each panel. Band intensities are averages of 3 independent RT-PCR reactions with SD.
doi:10.1371/journal.ppat.1002478.g006

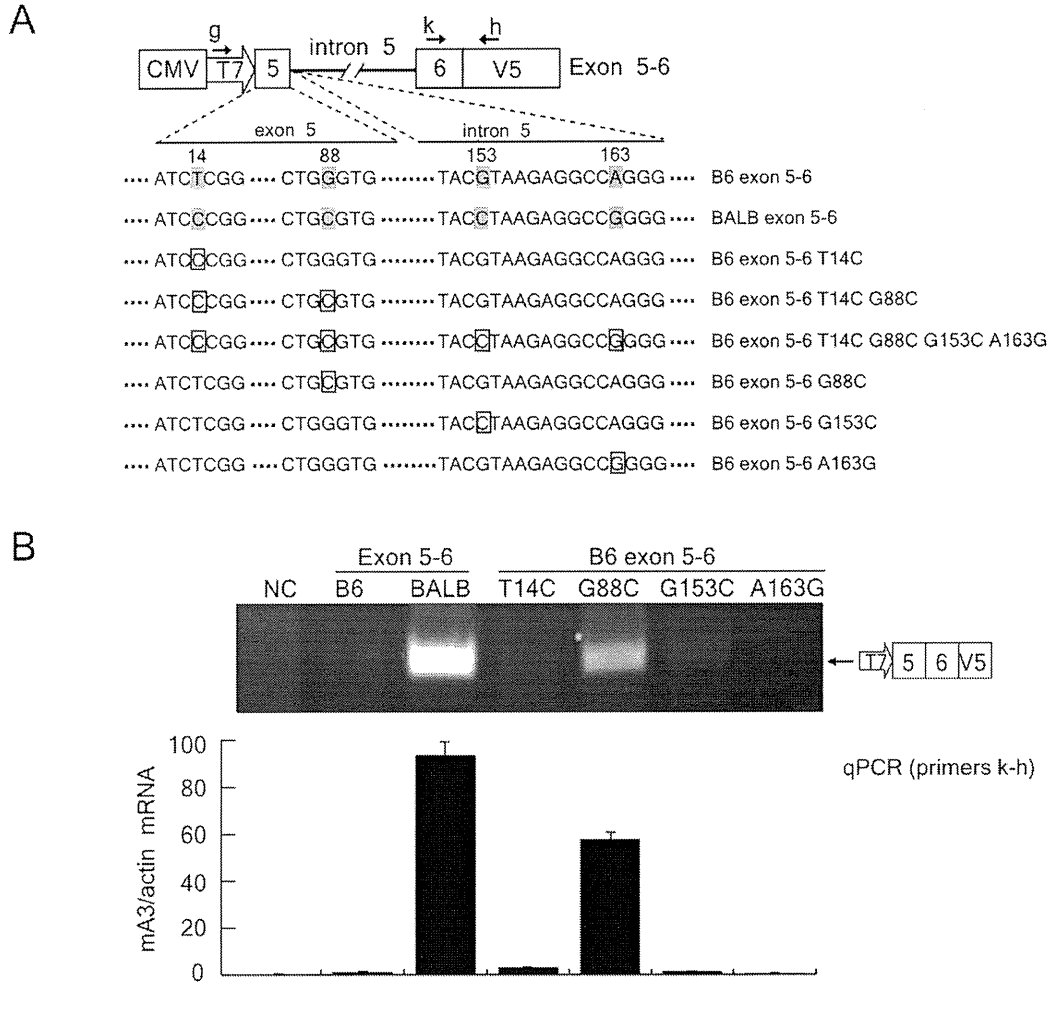
A
g
k
h
CMV
T7
5
intron 5
6
V5
Exon 5-6
exon 5
intron 5
14
88
153
163
.... ATCTCGG .... CTGGGTG ..... TACGTAAGAGGCCAGGG .... B6 exon 5-6
.... ATCCCGG .... CTGCGTG ..... TACCTAAGAGGCCGGGG .... BALB exon 5-6
.... ATCCCGG .... CTGGGTG ..... TACGTAAGAGGCCAGGG .... B6 exon 5-6 T14C
.... ATCCCGG .... CTGCGTG ..... TACGTAAGAGGCCAGGG .... B6 exon 5-6 T14C G88C
.... ATCCCGG .... CTGCGTG ..... TACCTAAGAGGCCGGGG .... B6 exon 5-6 T14C G88C G153C A163G
.... ATCTCGG .... CTGCGTG ..... TACGTAAGAGGCCAGGG .... B6 exon 5-6 G88C
.... ATCTCGG .... CTGGGTG ..... TACCTAAGAGGCCAGGG .... B6 exon 5-6 G153C
.... ATCTCGG .... CTGGGTG ..... TACGTAAGAGGCCGGGG .... B6 exon 5-6 A163G

B
Exon 5-6
B6 exon 5-6
NC
B6
BALB
T14C
G88C
G153C
A163G
T7
5
6
V5
100
80
60
40
20
0
mA3/actin mRNA
qPCR (primers k-h)

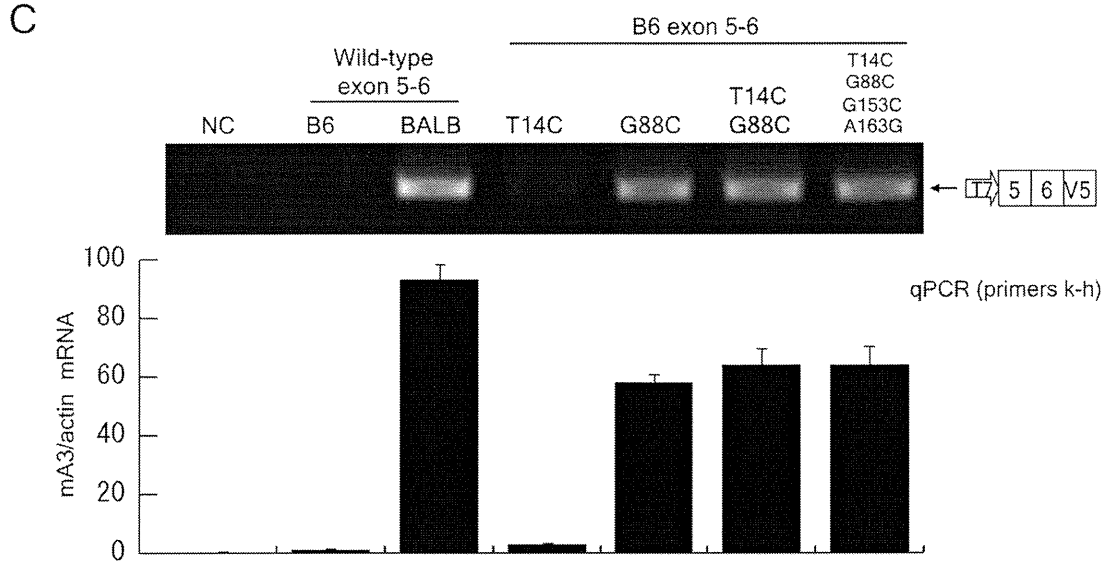
C
B6 exon 5-6
Wild-type exon 5-6
NC
B6
BALB
T14C
G88C
T14C G88C
T14C G88C G153C A163G
T7
5
6
V5
100
80
60
40
20
0
mA3/actin mRNA
qPCR (primers k-h)

Figure 7. The G88C nucleotide substitution in exon 5 is most critical for exon 5 inclusion into mA3 mRNA. (A) Polymorphic nucleotides indicated with the shades were exchanged between the B6 and BALB/c alleles at the sites indicated with the boxes. Plasmids used here carry the entire intron 5 instead of the deleted one used in the experiments shown in Figure 6. (B and C) The results of splicing assays using the plasmids depicted in panel (A). The predicted splicing product is shown on the right side of each panel. RT-PCR assays were performed with primers g and h. A portion of the transfected cells were utilized for luciferase assays to compare transfection efficiencies among the samples. Comparable levels of luciferase activities were observed in all samples in each experiment (data not shown). Quantitative real-time PCR data show averages of three reaction wells and SD.
doi:10.1371/journal.ppat.1002478.g007

Distribution of the TCCT repeat and G/C88 polymorphism among *Mus* species

Because the inclusion of exon 5 into mA3 message depends on the intron 4 TCCT repeat and the exon 5 G/C polymorphism at position 88 (G/C88), we screened additional inbred strains and wild mouse species for these sequence variations and for the presence or absence of exon 5 in the mA3 message. We sequenced exon 5 and segments of the flanking introns from 39 mice that represent different taxa or members of the same species trapped in different geographic locations (Table S1), as well as those from the inbred laboratory strains B10.A and A/WySn, prototypic strains with FV-restrictive and -permissive phenotypes [26,27,31,32]. The complete dataset is shown in Figure S1. Genomic sequencing showed that A/WySnJ mice share the TCCT duplication and exon 5 C88 SNP with BALB/c, while B10.A mice are identical to B6 mice at both sites (Figure 9A); this is consistent with previous observations on mA3 expression levels and inclusion of exon 5 in these strains of mice [27]. Among the 39 wild mice, the TCCT duplication was found in 10 mice that possessed the exon 5 C88 SNP, and all of the 29 other mice with G88 had a single TCCT copy as representatively shown in Figure 9A. The observed linkage between the repeated TCCT and C88 is reasonable, as both are required for efficient expression of 5+ message from the BALB/c allele (Figures 4, 6, and 8). RNA samples from 23 of the above mice were typed for the splicing phenotype. The presence or absence of exon 5 in mA3 mRNA correlated with the above identified sequence polymorphisms: exon 5 was present only in 7 mice, all of which had the linked TCCT duplication and C88, consistent with our functional assays. On the other hand, there were at least 7 discrepancies with respect to exon 5 inclusion and the C14 SNP confirming that this SNP has no major role in exon 5 splicing.

The coding sequence for exon 5 was present in all 39 *Mus* DNA specimens, as well as in rat DNA specimens (GenBank EDM15775) as described previously [29]. There were frameshift mutations within exon 5 in *M. setulosus* and both *M. cervicolor* subspecies, all of which lack exon 5 in mA3 mRNA, and the exon 5-containing splice variant was found only in mA3 mRNA of *M. spretus* and 3 of the house mouse species (*M. domesticus*, *M. musculus*, *M. castaneus*) (Figure 9B). The wild mice were also tested for the presence or absence of another genetic variation associated with variable expression levels of mA3, the exon 2-associated xenotropic MuLV LTR insertion [37]. Results indicated that the presence of this LTR (LTR^+), like the inclusion of exon 5 due to the above allelic variation (exon 5^+), was introduced into the *Apobec3* locus at about the time of the house mouse radiation (Figure 9B). These two features are not found together in any mouse, and the LTR^+ and exon 5^+ variants are both found in mice classed as *M. musculus* or *M. domesticus*, while *M. castaneus* mice have both variants as well as the ancestral $\Delta 5$ LTR^- mA3 type.

To better understand this species distribution, we typed additional samples of European *M. domesticus* and *M. musculus* for the presence of the LTR and exon 5 (Figure 9C). The geographic distribution of the trapping sites for these 19 house mice and for the exon 5^+ *M. spretus* indicated that the exon 5^+ mA3 was characteristic of *M. domesticus* of north Africa and western Europe, whereas LTR^+ mA3 was found in eastern Europe ($P = 0.049$ by Fisher's exact test). Four of the 9 eastern European *M. musculus* mice carried the *M. domesticus* variant, which is consistent with previous reports that gene flow across the hybrid zone is biased in the direction from *M. domesticus* to *M. musculus* ([42], for example). Additional samples identified as *M. domesticus* were trapped in the Americas (HAF, CL, WSA, PGN2, SC1, BQC, SAF, JJD, PERA; see Table S1), and these carried either the exon 5^+ mA3 (like *M. domesticus*) or the LTR^+ mA3 (like *M. musculus*); this is likely due to the fact that *Mus* are non-native species that were introduced into the Americas by passive transport, and although generally classed as *M. domesticus*, these mice show evidence of hybridization with other introduced house mouse species [43,44].

Discussion

Polymorphisms in mA3 are responsible for the fact that the B6 and C57BL/10 mouse strains are more restrictive to the replication of both beta- and gammaretroviruses than the BALB/c and A strains [25–29]. These differences in mA3 antiviral activities have been associated with sequence differences in the N-terminal region of mA3 [27], different levels of its mRNA expression [27,29,38,39], and the presence or absence of exon 5 in mA3 mRNA and protein [27], although the relative importance of these three factors for antiviral activity has not been established. In the present study, we focused on the role of exon 5 and have shown that the $\Delta 5$ mRNA directs more efficient mA3 protein synthesis than the exon 5-containing message. We have also identified 2 genetic determinants responsible for the inclusion of this exon into mA3, a TCCT repeat in intron 4 and a C88 substitution in exon 5 relative to the B6 allele. We further showed that these two determinants were coordinately acquired within the last 0.5 million years by house mouse species of *Mus*.

Previous studies have recognized differences in mRNA expression levels of mA3 between B6 and BALB/c mice [27,29,38,39]. Higher constitutive expression of mA3 mRNA is thought to contribute to better antiviral activity as suggested by the facts that higher levels of protein production result in more efficient incorporation of mA3 into viral particles [45] and that lipopolysaccharide (LPS)-induced enhancement of mA3 expression results in better restriction of MMTV *in vivo* [46]. It has also been shown that increased APOBEC3G and APOBEC3F expression is associated with lower viral load in rhesus macaques infected with simian immunodeficiency virus [47]. Higher protein levels of hA3G in $CD14^+$ monocytes are also associated with HIV-1-exposed but uninfected status in humans [48]. The increased level of *Apobec3* gene transcription has been associated with the presence in the B6 allele of an intact MuLV LTR, a sequence capable of driving enhanced transcription [37]. While increased levels of the mA3 transcript could be solely responsible for the presently observed increase in mA3 protein levels in B6 mice (Figure 1D), it was also reported that, when driven by the same strong promoter, the B6 mA3 cDNA lacking exon 5 produced more protein product than the exon 5-containing BALB/c cDNA and resulted in more efficient incorporation into viral particles

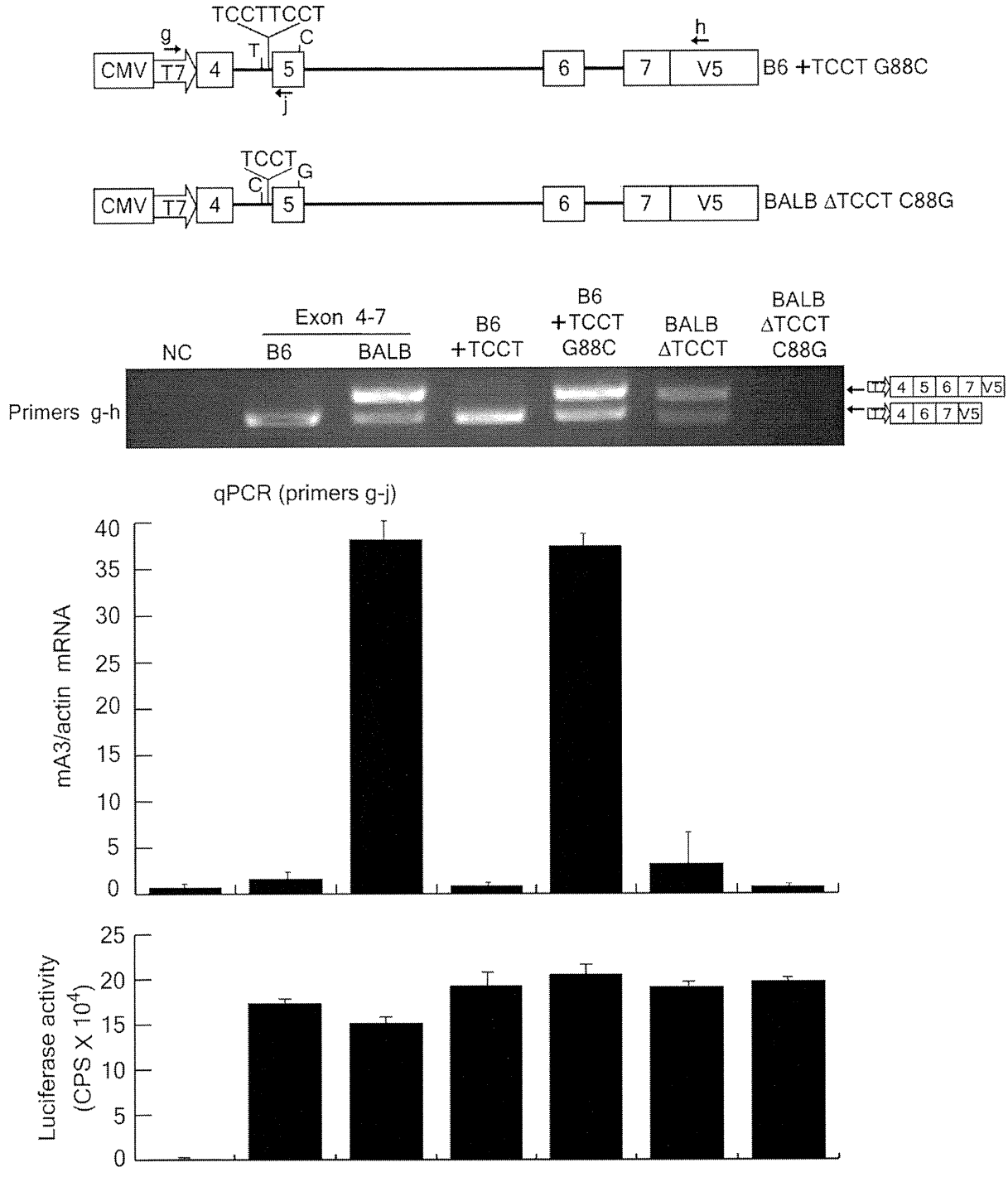

Figure 8. Effect of the combination of intron 4 TCCT repeat and exon 5 G/C SNP on exon 5 inclusion into the mA3 transcripts. B6 exon 4–7 + TCCT and BALB/c exon 4–7 ΔTCCT plasmids, as described in Figure 4, were further modified so that the exon 5 G/C SNP nucleotide at position 88 was reciprocally exchanged. The resultant plasmids were used for *in vitro* transcription assays as described for Figures 4–7. RT-PCR assays were performed with primers g and h. A portion of the transfected cells were utilized for luciferase assays to compare transfection efficiencies among the samples. Quantitative real-time PCR data show averages of three reaction wells and SD.
doi:10.1371/journal.ppat.1002478.g008

[27,45]. Thus, it was unclear whether the experimentally observed increased translation was due to the lack of exon 5 in the B6 cDNA or to the other sequence differences that distinguish the two *Apobec3* alleles [27,37,38]. Here we have clearly shown that the Δ5 mRNA directs much more efficient protein synthesis than the 5+ mA3 mRNA regardless of other allelic differences (Figures 2 and

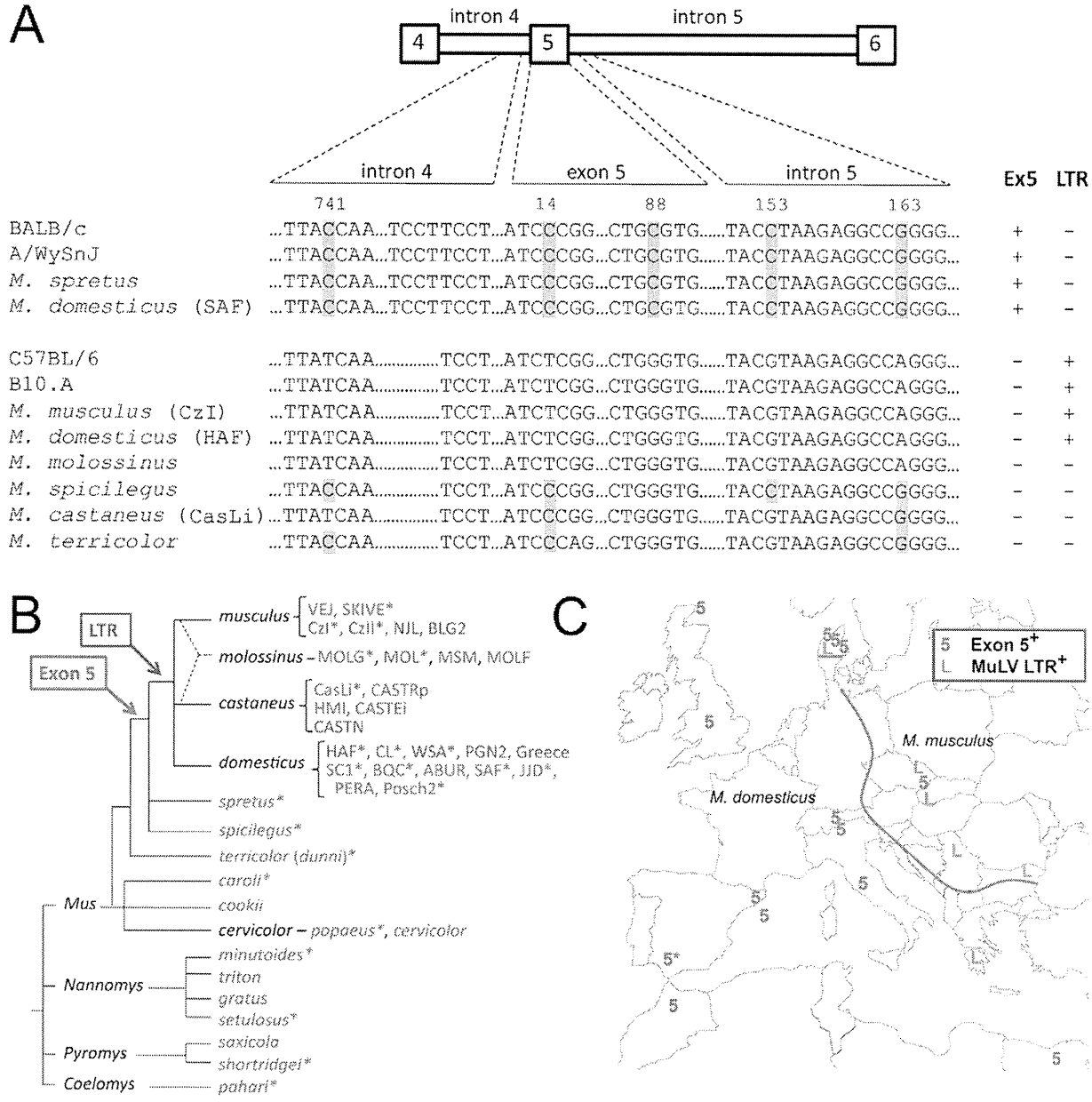

Figure 9. Distribution of sequence variations in and around the *Apobec3* exon 5 in *Mus* species and strains. (A) The *Apobec3* genomic sequences of the indicated strains and representative species are shown. The five SNP tested for their effects on exon 5 splicing are indicated with shaded bars. Also shown are the number of TCCT repeats and typing results indicating the presence or absence of exon 5 (Ex5) in spliced messages and the presence or absence of an MuLV LTR in intron 2. (B) The phylogenetic tree is a synthetic tree adapted from other sources [66–68]. Species are grouped into the 4 *Mus* subgenera and are listed to the right of each branch. Subspecies and stock or inbred line designations are given where multiple samples of a given species were tested. Red, exon 5^{+}/MuLV LTR^{-}; blue, Δ5/MuLV LTR^{+}; green, Δ5/MuLV LTR^{-}. *, mice tested for exon 5 splicing pattern. All were sequenced across exon 5 (Figure S1); PERA and MOLF sequence information was taken from Okeoma et al. [38]. (C) Distribution of expression variants of mA3 in mice trapped in Europe. The red line represents the 20 km-wide hybrid zone separating the ranges of *M. domesticus* and *M. musculus*. Symbols representing mA3 allelic variants are placed at trapping sites.
doi:10.1371/journal.ppat.1002478.g009

3), and the combination of the higher mRNA expression levels with preferential generation of the Δ5 isoform in mRNA splicing results in much higher mA3 protein levels in B6 in comparison with BALB/c mice (Figure 1).

The mechanisms by which the presence of exon 5 in the mRNA interferes with protein synthesis are currently unclear: however, predictions of the secondary structure for the mA3 mRNA suggest that the portion encoding exon 5 may form stable stem-loop structures (Figure S2), which might interfere with efficient translation. The predicted stem-loop structure is thermodynamically more stable for B6 than for BALB/c exon 5, and this portion is actually spliced out from the major transcript in B6 mice. It is

possible, therefore, that the elimination of this exon from mA3 mRNA confers a functional advantage to B6 mice through more efficient translation of the Δ5 mRNA and resultant higher levels of mA3 protein expression. It should be noted, however, that introduction of this exon between the two CDDs does not physically disrupt the functional domains, as the 5+ product of the BALB/c allele still exerts deaminase activity and restricts AKV replication *in vitro* [29]. The possible effect of this 33-amino acid exon on interactions between the N-terminal and C-terminal CDDs and on mA3 oligomerization remains to be elucidated.

Our results also show that the ancestral *Mus Apobec3* gene locus lacked both the MuLV LTR and the functional polymorphisms that determine exon 5 inclusion (Figure 9). These two genetic features were acquired independently at about the time of the house mouse radiation 0.5–1.0 million years ago, and are found in distinct lineages of wild mice and different inbred strains of laboratory mice. It should be noted that all 4 house mouse species originated and diverged from an ancestral population on the Indian subcontinent that carries many of the alleles found in peripheral Eurasian populations [49,50]. The observed distribution of the LTR^+ and exon 5^+ mA3 variants among the house mouse lineages is consistent with the appearance of these variants in this ancestral population. It is thus likely that *M. domesticus* progenitors carrying the exon 5^+ *Apobec3* allele moved west to north Africa and western Europe, and *M. musculus* (LTR^+) moved north to Russia, eastern Europe and north China. *M. castaneus*, which carries these two variants as well as the ancestral Δ5 LTR^- mA3, migrated east to Thailand and China. Only the ancestral mA3 type is found in *M. molossinus*, which is a natural hybrid of *M. musculus* and *M. castaneus* [44], and these Japanese mice presumably inherited their *Apobec3* gene from their *M. castaneus* progenitors.

Numerous studies indicate that host antiviral factors co-evolve with the pathogens they restrict, and this "arms race" is responsible for mutational changes in APOBEC3 in primates and mice as evidenced by detectable positive selection [37,51]. The acquisition of the MuLV LTR that is associated with enhanced mA3 transcription in virus-infected mice also makes sense as an evolutionary adaptation to pathogen infection [37]. Thus, the B6 *Apobec3* allele has acquired two advantageous features that contribute to enhanced retrovirus restriction: high mRNA expression directed by the intron 2 LTR that is in linkage with the positively selected, more functional amino acid sequence in the N-terminal deaminase domain [27,37]. The BALB/c allele, in contrast, acquired the polymorphisms that direct exon 5 inclusion as shown in the present study, along with coding sequence polymorphisms associated with lower antiviral activity [27]. The far-flung distribution of exon 5^+ mA3 throughout western Europe (Figure 9C) is surprising, because this allele, having a reduced level of mA3 protein expression with inefficient restriction of MuLV replication at least *in vitro* [27], would seem to be evolutionarily deleterious. The observed distribution of exon 5^+ mA3 suggests either that the exon 5^+ variant provides sufficiently protective levels of antiviral activity in virus-infected mice and is therefore not subject to purifying selection, that these particular mice have not been exposed to significant challenge by mA3-sensitive pathogens, that this mA3 variant provides some other, unrecognized selective advantage, or that this allele is tightly linked to another advantageous polymorphism.

All 4 house mouse species possessing the exon 5^+ genetic variation carry beta- and gammaretroviruses along with other retroelements that are subject to APOBEC3 restriction [25–30,52]. In this regard, although the BALB/c mA3 is less antiviral than the product of the B6 allele, it does have measurable antiviral activity [29]. Further, analysis of 54 germline MuLV proviruses of three envelope types in the sequenced B6 genome demonstrated evidence of APOBEC3-mediated editing of the polytropic and modified polytropic, but not the xenotropic, proviruses [30]. The mA3-edited polytropic and modified polytropic viruses originated in *M. domesticus* [52,53], mice that carry the exon 5^+ mA3, suggesting that this mA3 variant may be effectively antiviral *in vivo*. Finally, in mA3-deficient B6 mice, the absence of this protein differentially affects FV replication depending on target cell types [54]. As cell type-dependent and pathogen-induced changes in mA3 expression may differ between mice of the ancestral Δ5 LTR^-, exon 5^+, and LTR^+ variants, mice with the exon 5^+ *Apobec3* allele may still restrict mA3-sensitive pathogens in critical target cells.

It is also possible that some mA3 polymorphisms have been selected for reasons other than their antiviral functions, and these functions may take precedence in mice not threatened with retrovirus assault. It is unlikely that differences in mA3 expression levels and/or its amino acid sequence provide a significant selective advantage in terms of normal development, survival, or fertility, as *Apobec3*-knockout mice show no increased propensity for tumor development or disease, and both male and female mA3-deficient mice were fertile [40]. On the other hand, the presence of active cytidine deaminases can have costs that may become more significant when endogenous and exogenous retroviral activity is low. Transgenic mice overexpressing mouse activation-induced deaminase (AID) or rabbit apolipoprotein B mRNA-editing enzyme catalytic polypeptide 1 (APOBEC1), two other members of the AID/APOBEC family of cytidine deaminases, developed neoplastic diseases and showed evidence of significant editing of various expressed genes [55,56]. This suggests that when the retroviral threat is low, the consequences of possessing highly active mutagenic enzymes, like the Δ5 mA3 expressed in B6 mice, can outweigh their advantages as antiviral factors. In this regard, it should be noted that infectious MuLV has not been isolated from European *M. domesticus*, which carry the less highly expressed 5+ mA3, whereas the more active *Apobec3* alleles are found in all 3 of the other species of *Mus*, all of which have been found to carry infectious MuLVs [57].

Finally, it has also been observed that there is a similarly widespread distribution in humans of a deletion of a genomic segment harboring the *Apobec3b* gene locus [58]. At least one copy of this deletion is present in >40% of humans. The selective advantage of this genetic variant has not been determined, but its retention may suggest a possible advantage in reducing the genotoxic activity of this cytidine deaminase, or alternatively, it may be linked to positively selected variants in one or more of the 6 linked human APOBEC3 paralogues [59,60]. Further comparative analyses of the geographic and species distributions of natural mouse pathogens and the various mA3 variants may help define previously unrecognized targets of APOBEC3-mediated restriction and provide further insight into the coevolution of pathogens and this host restriction factor.

Materials and Methods

Ethics statement

The studies utilizing laboratory animals were carried out in strict accordance with the Act on Welfare and Management of Animals of the government of Japan and the Regulations for the Care and Use of Laboratory Animals of Kinki University. The protocol was approved by the Institutional Animal Experimentation Committee of Kinki University School of Medicine (Permit Number: KAME-19-029). All surgery was performed under sodium pentobarbital anesthesia, and all efforts were made to

minimize suffering. All studies involving wild mice were performed in compliance with the US Government Principles for the Utilization and Care of Vertebrate Animals used in Testing, Research, and Training; the Public Health Service Policy on Humane Care and Use of Laboratory Animals; The Animal Welfare Act and amendment laws; the Animal Care Policies of the USDA; The Guide for the Care and Use of Laboratory Animals (7th Edition; National Research Council); and the guidelines of the Committee on the Care and Use of Laboratory Animals under an NIAID-approved animal study protocol, and all studies and procedures were reviewed and approved by the Institutional Animal Care and Use Committee of the NIH (Permit Number: ASP LMM 1).

Mice and mouse genomic DNA

C57BL/6NCrslc, BALB/cCrslc, and B10A/SgSnslc mice were purchased from Japan SLC, Inc., Hamamatsu, Japan. Breeding pairs of A/WySnJ mice were purchased from The Jackson Laboratory, Bar Harbor, ME. The mA3-deficient strain on the B6 background has been described [27,40]. All laboratory mice were housed and bred in the Experimental Animal Facilities at Kinki University School of Medicine under specific pathogen-free conditions. The isolation of genomic DNA from spleens was carried out with DNeasy blood and tissue kit (Qiagen, Inc., Hilden, Germany) according to the manufacturer's instructions.

DNA and RNA were separately isolated from animals and cell lines developed from wild mice and wild mouse-derived breeding colonies or inbred strains (Table S1). Many wild-derived mice were obtained from M. Potter (National Cancer Institute, Bethesda, MD). CAST/Rp mice were obtained from R. Elliott (Roswell Park Cancer Institute, Buffalo, NY). Cells from some wild mouse species were obtained from J. Rodgers (Baylor College of Medicine, Houston, TX) and from J. Hartley, M. Lander or S. Chattopadhyay (National Institute of Allergy and Infectious Diseases, Bethesda, MD) [61,62]. *M. cervicolor popaeus* mice and tissue samples were obtained from R. Callahan (National Cancer Institute). Mice or DNA samples of inbred lines of *M. castaneus* (CAST/EiJ) and *M. molossinus* were obtained from The Jackson Laboratory. *M. musculus* DNA samples were obtained from S. Chattopadhyay and H. Morse (National Institute of Allergy and Infectious Diseases). DNA samples from wild-trapped European *M. domesticus* were provided by M. Nachman (University of Arizona, Tucson). DNA samples from 5 wild-derived strains (BLG2, NJL, MSM, HMI, PGN2) were obtained from the National Institute of Genetics, Mishima, Japan. A set of *Nannomys* DNAs was obtained from Y. Cole and P. D'Eustachio (Departments of Biochemistry and Medicine, New York University, NY); these mice were classed into 4 species on the basis of skeletal features by J. T. Marshall (Smithsonian Natural History Museum, Washington, DC). DNA was isolated from cultured tail biopsies, spleen, or liver by standard protocols, and RNA was isolated from the spleen or liver using TRI-Reagent (Molecular Research Center, Cincinnati, OH) or by a guanidine chloride extraction method [63].

Mouse *Apobec3* sequences and the prediction of mRNA secondary structures

DNA containing the mouse *Apobec3* exon 5 and associated intron sequences was amplified using either one of the following forward primers: 5′-GGACAATGGTGGCAGGCGATTC-3′, 5′-GCATCTTTGTGGATGGGG-3′, and the reverse primer 5-TCATTCCTCAATGCTCCTCC-3′. PCR products were cloned into pCR2.1-TOPO (Invitrogen, Carlsbad, CA) before sequencing. The *Apobec3* region was amplified from genomic DNA of B6, BALB/c, B10A, and A/WySnJ mice using the forward primer 5′-TTACAAATTTTAGATACCAGGATTCTAAGCTTCAGG-AG-3′ and the reverse primer 5′-GTCCTTTATGTGGGTTC-CAAGGACC-3′. PCR products were treated with ExoSAP-IT (USB, Cleveland, OH) and directly sequenced with the above reverse primer. To determine the BALB/c genomic sequence of the *Apobec3* intron 5, the BALB exon 5–6 and BALB intron 5-Δ3′ plasmids (Figure 5) were sequenced by using BigDye Terminator V3.1 Cycle Sequencing Kit (Applied Biosystems, Foster City, CA) and an ABI PRISM 3100 Genetic Analyzer (Applied Biosystems) using the following primers: T7 promoter forward, 5′- TAATAC-GACTCACTATAGGG-3′; and V5 reverse, 5′-CGTAGAATC-GAGACCGAGGAGAGGGTTAGGGATAGGC-3′.

The secondary structure of a portion of the mA3 mRNA exon 5 was predicted with *mfold* [64,65].

Cell culture and DNA transfection

BALB/3T3 and human 293T cells were cultured in Dulbecco's modified Eagle medium supplemented with 10% heat-inactivated fetal bovine serum (Invitrogen). These cells were seeded at 1.0×10^5/well in a well of 6-well plates one day prior to transfection. DNA transfection was performed by using Lipofectamine 2000 (Invitrogen) according to the manufacturer's protocols. Mouse spleen cells were harvested as described previously for protein and RNA extractions [27]. At least three independent transfection experiments were performed in this study and representative results are shown in the figures.

Plasmid constructions

The expression plasmids, pFLAG-CMV2-*mA3*^{b}Δ5 harboring the mA3 cDNA derived from the Δ5 transcript of the B6 allele, pFLAG-CMV2-*mA3*^{d} harboring the cDNA derived from the 5+ transcript of the BALB/c allele, pFLAG-CMV2-*mA3*^{d}Δ5 harboring the cDNA derived from the Δ5 transcript of the BALB/c allele, and control pFLAG-CMV2-GFP have been described [27]. The genomic DNA encoding the mA3 exon 5 was amplified from B6 genome with the following primers: 5′-ACCTTGCTACATCTCGGTCCCTTC-CAGC-3′ and 5′-CTGCCCTCCACCCAGAACCTCGTCTC-TGG-3′. The above pFLAG-CMV2-*mA3*^{b}Δ5 was used as a PCR template with primers 5′-GCGAATGGACCCGCTAAGTGAA-GAGG-3′ and 5′-CTCAGAATCTCCTGAAGCTTAGAATCC-TGG-3′ to amplify the linearized plasmid with a gap between exons 4 and 6. The two PCR products above were treated with T4 polynucleotide kinase (TAKARA Bio, Otsu, Japan) and fused by using the DNA Ligation Kit ver.2.1 (TAKARA Bio) to construct the plasmid pFALG-CMV2-*mA3*^{b}, which expresses the 5+ mA3 cDNA derived from the B6 allele.

B6 or BALB/c genomic fragments harboring exons 4–7 and the intervening introns were amplified by PCR using either the B6 or BALB/c genomic DNA as a template and the common primers 5′-CACCAATTTAAAAAGTGTTGGAAGAAG-3′ and 5′-GTGGGAGGTCCATGACGTCCACCAGGATCCC-3′. Each amplified DNA product was cloned into a pcDNA3.2/V5/GW/D-TOPO cloning vector (Invitrogen) and designated as B6 or BALB exon 4–7, respectively. The above B6 or BALB exon 4–7 was used as a template with the primers 5′-CACCACCTTGC-TACATCTCGGTCC-3′ and 5′-GCAGAGATGCTTGACTC-GTTGGTTG-3′ or 5′-CACCACCTTGCTACATCCCGGTC-C-3′ and 5′-GCAGAGATGCTTGACTCGTTGGTTG-3′, respectively, for the amplification of B6 or BALB/c exons 5 and 6 and the intervening intron 5. Each PCR product was cloned into the pcDNA3.2/V5/GW/D-TOPO vector and designated as B6 or BALB exon 5–6. The DNA fragments harboring sequentially deleted *Apobec3* intron 5 were prepared by PCR using either one of the above B6 or BALB exon 5–6 plasmids as a common template

with the primer pairs A–F listed in Table S2. Each amplified DNA product was cloned into the pcDNA3.2/V5/GW/D TOPO vector to generate the expression plasmid shown in Figure 5B.

Reciprocal chimeras between the above B5 and BALB exon 5–6 plasmids were generated by amplifying a linearized plasmid DNA lacking the 3′ intron 5 and exon 6 using primer pair G, and by amplifying the insert fragment using primer pair H.

Site-directed mutagenesis was performed by employing the QuikChange Site-Directed Mutagenesis Kit (Stratagene, La Jolla, CA) using the following templates and primers, listed separately in Table S2: BALB 100bp intron 5 (3′-100bp) plasmid was used as a common template for the preparation of BALB C14T, BALB C88G, and BALB C153GG163A with primer pairs I, J, K, respectively: B6 100bp intron 5 (3′-100bp) plasmid was used as a template to make B6 T14C or B6 G88C with primer pair L or M, respectively. The resultant B6 T14C plasmid was used as a template with the same primer pair M employed for the generation of B6 G88C to make B6 T14C G88C. B6 T14C G88C was then used as a template for the generation of B6 T14C G88C G153C A163G by using primer pair O. Similarly, the above-used primer pairs were also utilized for the generation of B6 exon 5–6 T14C, B6 exon 5–6 T14C G88C, and B6 exon 5–6 T14C G88C G153C A163G mutants by using B6 exon 5–6 as a template. The B6 exon 5–6 plasmid was also used as a template with primer pairs M, P, and Q for making B6 exon 5–6 G88C, B6 exon 5–6 G153C, and B6 exon 5–6 A163G, respectively.

To make BALB ΔTCCT, 4 consecutive nucleotides within the repeat sequence, TCCT, were deleted from the BALB exon 4–7 plasmid by mutagenesis using primer pair R, listed in Table S2. BALB ΔTCCT or BALB exon 4–7 plasmid was used as a template with primer pair S to make BALB C741T ΔTCCT or BALB C741T, respectively. To introduce the TCCT sequence by mutagenesis and make B6+TCCT, B6 exon 4–7 plasmid was used as a template with primer pair T. B6+TCCT or B6 exon 4–7 was used as a template with primer pair U to generate B6 T741C+TCCT or B6 T741C, respectively. Similarly, the above produced B6 exon 4–7+TCCT or BALB exon 4–7 ΔTCCT plasmid was used as a template and G88C or C88G substitution was introduced with primer set M or J, respectively.

All resultant plasmids were entirely sequenced by using BigDye Terminator V3.1 Cycle Sequencing Kit with an ABI PRISM 3100 Genetic Analyzer. In order to normalize the transfection efficiency, a plasmid expressing the luciferase gene, p*luc,* based on the expression vector pGL3 (Promega, Madison, WI), was utilized. All the primers used in this study were purchased from Operon Biotechnologies, Tokyo, Japan.

Quantitative real-time PCR assays for endogenous mA3 transcripts

For the quantification of mA3 transcripts in mouse spleens, total RNA was extracted from each spleen with RNeasy Mini Kit (Qiagen). The RNA was then subjected to reverse transcription with PrimeScript RT reagent Kit (TAKARA Bio). Real-time PCR reactions were carried out with SYBR Premix Ex Taq II (TAKARA Bio) on an Applied Biosystems 7900HT Fast Real-Time PCR System (Applied Biosystems) with two different sets of *Apobec3*-specific primers: set 1, 5′-GTGTTGGAAGAAGTTT-GTGG-3′ (primer a) and 5′-CCTGAAGCTTAGAATCCTGG-3′ (primer b); and set 2, 5′-TTACAAATTTTAGATACCAG-GATTCTAAGCTTCAGGAG-3′ (primer c) and 5′-TTGGTT-GTAAAACTGCGAGTAAAATTCCTCTTCAC-3′ (primer d). The data were normalized with expression levels of β-actin mRNA to obtain ΔCt values, and ΔΔCt values were calculated.

Detection and quantification of the *mA3* transcripts and their splicing products

For the detection of endogenous mA3 transcripts in mouse spleen cells, the RT products and primer sets used for the real-time PCR were also utilized for PCR using KOD Dash DNA polymerase (Toyobo, Osaka, Japan). The PCR products were separated by 1% agarose gel electrophoresis and detected by staining with ethidium bromide. For splicing assays, BALB/3T3 cells were transfected with 1 μg of each plasmid harboring a genomic DNA fragment and 0.5 μg of p*luc* to normalize the transfection efficiency. Total RNA was extracted from the transfected cells using the RNeasy Mini Kit at 24 hours post-transfection. The total RNA was treated with DNase I, reverse transcribed with SuperScript III First Strand Synthesis System (Invitrogen), and the resultant cDNA was subjected to PCR detection using KOD Dash DNA polymerase with the following primers: 5′-TAATACGACTCACTATAGGG-3′ (primer g) and 5′-CGTAGAATCGAGACCGAGGAGAGGGTTAGGGATAG-GC-3′ (primer h), designed to hybridize the T7 promoter and V5 tag regions of the vector, respectively. Primer i, 5′-GGTC-TCCCAGAGACGAGGTTCTG-3′, was used to detect only the exon 5-containing transcript. For real-time PCR quantification of the *mA3* transcripts containing exon 5, primer j (5′-GTGGAT-GAAGAGCTGGAAGGGACCG-3′) was used along with the above primer g. Transcripts containing exon 6 were similarly quantified by using primer k (5′-CAACCAACGAGTCAAG-CATCTCTGC-3′) and the above primer h.

For RT-PCR detection of mA3 mRNA in cells transfected with an mA3 expression plasmid, the same RT product as was used for real-time PCR analyses was utilized with the above-described primer set 1 (a–b). The RT products made by PrimeScript RT reagent Kit were supposed to be relatively short in length because a mixture of oligo-dT and random 6-mers were used as primers in the RT reaction. Thus, in order to detect the full-length and Δ5 transcripts, the following primers, 5′-GGGAATTCGATGG-GACCATTCTGTCTGGGATGCAGCCATCGC-3′ (primer e) and 5′-GGGTCGACTCAAGACATCGGGGGTCCAAGCTG-TAGGTTTCC-3′ (primer f), were used along with newly synthesized RT products generated by the SuperScript III First Strand Synthesis System (Invitrogen). To quantify the mA3 transcripts in 293T cells transfected with an mA3 expression plasmid, one-third of the transfected cells were used for total RNA isolation using the RNeasy Mini Kit at 24 hours after transfection. The purified RNA was treated with 5 units of DNase I (TAKARA Bio) for 1 hour at 37°C to digest the transfected DNA and then reverse transcribed with the PrimeScript RT reagent Kit. The real-time PCR was performed as described above.

For RT-PCR analyses of mA3 transcripts generated by the *in vitro* transcription/translation system, the reaction was stopped by the addition of lysis buffer included in RNeasy Mini Kit after 30 or 60 min of incubation, and the transcribed products were purified with the above kit. After the treatment of the purified RNA with DNase I, the RT-PCR reaction was carried out with the above primer set 1. After electrophoresis, gel images were recorded with a FluorChem™ IS-8900 transilluminator and band intensities were analyzed with AlphaEase FC Stand Alone software (Alpha Innotech, San Leandro, CA).

Apobec3 splicing patterns for wild-derived mice were identified by RT-PCR to amplify a segment of mA3 RNA spanning exon 5 from total RNA using forward primer 5′-GGACCATTCTG-TCTGGGATGCAGCCATCG-3′ and reverse primer 5′-GG-TTGTAAAACTGCGAGTAAAATTCC-3′.

Luciferase assays

Luciferase assays for normalization of transfection efficiencies were performed by utilizing the Luciferase Assay System (Promega). The enzymatic activities were measured by Wallac 1420 ARVO^{TM} MX-2 Multilabel Counter (Perkin Elmer).

Pre-absorption of the antibody

A spleen from an *Apobec3* knock-out mouse [40] was homogenized in 1ml ice-cold phosphate-buffered saline (PBS). Four ml of ice-cold acetone was added to the homogenate, mixed, and incubated on ice for 30 min. The lysate was centrifuged at 10,000×*g* at 4°C for 10 min. The pellet was washed with ice-cold acetone once and dried completely at room temperature to make spleen extract powder. Two µl of anti-APOBEC3 NT antibody specific for the N-terminal portion of mA3 (Millipore, Billerica, MA) was added to 0.5ml of KTBT buffer (50 mM Tris-HCl, pH 7.5, 150 mM NaCl, 10 mM KCl, 1% Triton X-100) containing 10% (w/v) unimmunized sheep serum as a carrier, into which 3mg of the spleen extract powder was dissolved. The mixture was incubated overnight at 4°C with gentle rotation. After centrifugation at 10,000×*g* at 4°C for 10 min, the supernatant was used as a pre-absorbed anti-mA3 antibody.

Immunoblotting

Western blotting analyses were conducted as described previously [27] with some modifications. Briefly, proteins were extracted with a lysis buffer (1% Nonidet P-40, 25 mM Tris-HCl, pH 7.5, 140 mM NaCl, 1 mM EDTA, 10 mM $Na_4P_2O_7$) containing protease inhibitors from Complete, Mini, EDTA-free Protease Inhibitor Cocktail Tablets (Roche Applied Science, Mannheim, Germany) and a phosphatase inhibitor, PhosSTOP (Roche Applied Science). Total protein concentrations were determined by Bradford assay (Nacalai Tesque, Kyoto, Japan) and the extracts were mixed with sodium dodecyl sulfate (SDS)-polyacrylamide gel electrophoresis (PAGE) sample buffer and heated at 95°C for 5 min. The proteins were separated by SDS-PAGE, transferred to Immobilon-P membrane (Millipore), and the blotted membranes were blocked with 5% (w/v) skim milk (Wako Pure Chemicals, Osaka, Japan) in Tris-buffered saline with 0.05% Tween 20 (TBST). The blocked membranes were incubated with the primary antibody at 4°C overnight. Membranes were then washed with TBST and incubated with horse radish peroxidase (HRP)-conjugated secondary antibody for 2 hours at room temperature, washed again with TBST, and the bound antibodies were detected using ECL plus reagent (GE Healthcare, Tokyo, Japan). The images were captured with a LAS-1000 Plus (Fujifilm, Tokyo, Japan) and the band intensities evaluated with Image Gauge ver. 3.12 (Fujifilm). A 1/5 dilution of the above-mentioned pre-absorbed mA3 antibody was made with IMMUNO SHOT (COSMO BIO, Tokyo, Japan) and was used as a primary antibody. Anti-FLAG M2 monoclonal antibody (mAb) (Sigma-Aldrich), anti-IκBα mAb (L35A5) (Cell Signaling Technology, Beverly, MA), anti-actin antibody (C-11) (Santa Cruz, CA), and the His-probe (H-15) (Santa Cruz) were diluted at 1:1000 with TBST. HRP-conjugated rabbit anti-mouse IgG (Zymed, South San Francisco, CA) and HRP-conjugated Goat anti-rabbit IgG antibodies (Invitrogen) were also diluted at 1:1000 and used as secondary antibodies to detect each appropriate primary antibody.

Assessment of mA3 protein stability

1.0×10^5 of 293T cells were transfected with 0.1 µg of an mA3 expression plasmid, 0.01 µg pFLAG-CMV2-GFP, and 0.1 µg of p*luc*. After 24h, the cells were treated with 10 µg/ml of cycloheximide or its solvent dimethyl sulfoxide (DMSO) as a control for 0, 2, or 4 hours. The cells were washed and resuspended in PBS. One-tenth of the cell suspension was subjected to luciferase assays to normalize transfection efficiencies, and the remaining cells were dissolved in the SDS-PAGE sample buffer. The normalized amount of cell lysates were separated by SDS-PAGE followed by immunoblotting as described above.

In vitro transcription and translation

The FLAG-mA3 cDNA was amplified with highly proofreading Pfu Turbo DNA Polymerase (Stratagene) from the plasmids pFLAG-CMV-*mA3^d* and pFLAG-CMV-*mA3^{d}Δ5* [27], with a forward primer harboring the T7 promoter sequence, 5′-GGATCCTAATACGACTCACTATAGGGAACAGCTGGGATGGGACCATTCTGTCTGGGATGC-3′ and a reverse primer harboring the His-Tag sequence, 5′-TCAATGGTGATGGTGATGATGAGCAGCAGCAGACATCGGGGGTCCAAGCTGTAGG-3′. The PCR products were subjected to reactions for *in vitro* transcription and translation using TNT T7 Quick for PCR DNA (Promega) according to the manufacturer's protocol. Half of the generated products were mixed with the SDS-PAGE sample buffer and analyzed by immunoblotting. The remaining products were used for RNA purification with RNeasy Mini Kit (Qiagen) followed by RT-PCR to detect mA3 transcripts.

Supporting Information

Figure S1 Nucleotide sequence of the genomic region encoding mA3 exon 5 and segments of flanking introns from several laboratory mouse strains and wild mouse species. Mouse *Apobec3* exon 5 and the flanking introns from 39 mice that represent different taxa or members of the same species trapped in different geographic locations, as well as those from the inbred laboratory strains BALB/c, B10.A, and A/WySn, were sequenced and aligned with the corresponding B6 sequence. The exon 5 and six key polymorphic regions, C/T741 and TCCT repeat in intron4, C/T14 and C/G88 in exon5, and C/G153 and A/G163 in intron 5, are indicated. Accession numbers for all newly obtained sequence data are also provided in this figure.
(PDF)

Figure S2 Possible stem-loop structures predicted from the mA3 intron 5 mRNA sequence. The mRNA secondary structures of exon 5 encoded by the B6 and BALB/c alleles were predicted by using the mfold [64,65]. Polymorphic nucleotides within this exon, U/C at position 14 and G/C at position 88, are indicated.
(PDF)

Table S1 Designations and sources of wild-derived mice, their cells, and DNA samples.
(PDF)

Table S2 Primers used to generate intron 5 deletion mutants and chimeras, for exon 5/intron 5 nucleotide substitutions, and for modification of TCCT repeat and T/C 741 SNP in intron 4.
(PDF)

Acknowledgments

We thank Drs. Sachiyo Tsuji-Kawahara, Eiji Kajiwara, and Shiki Takamura for their helpful discussions and comments and Mr. J. Brian Dowell for critically reading and correcting the manuscript. We thank Alicia Buckler-White for DNA sequencing. We are also grateful to the National Institute of Genetics, Mishima, Japan, for the provision of genomic DNA samples from wild mouse strains.

Author Contributions

Conceived and designed the experiments: MM. Performed the experiments: JL YH ET QL CAK. Analyzed the data: YI CAK MM. Contributed reagents/materials/analysis tools: CAK MM. Wrote the paper: YH CAK MM.

References

1. Bogerd HP, Wiegand HL, Doehle BP, Lueders KK, Cullen BR (2006) APOBEC3A and APOBEC3B are potent inhibitors of LTR-retrotransposon function in human cells. Nucleic Acids Res 34: 89–95.
2. Bogerd HP, Wiegand HL, Hulme AE, Garcia-Perez JL, O'Shea KS, et al. (2006) Cellular inhibitors of long interspersed element 1 and Alu retrotransposition. Proc Natl Acad Sci USA 103: 8780–8785.
3. Chen H, Lilley CE, Yu Q, Lee DV, Chou J, et al. (2006) APOBEC3A is a potent inhibitor of adeno-associated virus and retrotransposons. Curr Biol 16: 480–485.
4. Esnault C, Heidmann O, Delebecque F, Dewannieux M, Ribet D, et al. (2005) APOBEC3G cytidine deaminase inhibits retrotransposition of endogenous retroviruses. Nature 433: 430–433.
5. Esnault C, Millet J, Schwartz O, Heidmann T (2006) Dual inhibitory effects of APOBEC family proteins on retrotransposition of mammalian endogenous retroviruses. Nucleic Acids Res 34: 1522–1531.
6. Esnault C, Priet S, Ribet D, Heidmann O, Heidmann T (2008) Restriction by APOBEC3 proteins of endogenous retroviruses with an extracellular life cycle: *ex vivo* effects and *in vivo* "traces" on the murine IAPE and human HERV-K elements. Retrovirology 5: 75.
7. Harris RS, Bishop KN, Sheehy AM, Craig HM, Petersen-Mahrt SK, et al. (2003) DNA deamination mediates innate immunity to retroviral infection. Cell 113: 803–809.
8. Lochelt M, Romen F, Bastone P, Muckenfuss H, Kirchner N, et al. (2005) The antiretroviral activity of APOBEC3 is inhibited by the foamy virus accessory Bet protein. Proc Natl Acad Sci USA 102: 7982–7987.
9. Mangeat B, Turelli P, Caron G, Friedli M, Perrin L, et al. (2003) Broad antiretroviral defence by human APOBEC3G through lethal editing of nascent reverse transcripts. Nature 424: 99–103.
10. Mariani R, Chen D, Schrofelbauer B, Navarro F, Konig R, et al. (2003) Species-specific exclusion of APOBEC3G from HIV-1 virions by Vif. Cell 114: 21–31.
11. Navarro F, Bollman B, Chen H, Konig R, Yu Q, et al. (2005) Complementary function of the two catalytic domains of APOBEC3G. Virology 333: 374–386.
12. Russell RA, Wiegand HL, Moore MD, Schafer A, McClure MO, et al. (2005) Foamy virus Bet proteins function as novel inhibitors of the APOBEC3 family of innate antiretroviral defense factors. J Virol 79: 8724–8731.
13. Sasada A, Takaori-Kondo A, Shirakawa K, Kobayashi M, Abudu A, et al. (2005) APOBEC3G targets human T-cell leukemia virus type 1. Retrovirology 2: 32.
14. Schumacher AJ, Hache G, Macduff DA, Brown WL, Harris RS (2008) The DNA deaminase activity of human APOBEC3G is required for Ty1, MusD, and human immunodeficiency virus type 1 restriction. J Virol 82: 2652–2660.
15. Sheehy AM, Gaddis NC, Choi JD, Malim MH (2002) Isolation of a human gene that inhibits HIV-1 infection and is suppressed by the viral Vif protein. Nature 418: 646–650.
16. Turelli P, Mangeat B, Jost S, Vianin S, Trono D (2004) Inhibition of hepatitis B virus replication by APOBEC3G. Science 303: 1829.
17. Vartanian JP, Guetard D, Henry M, Wain-Hobson S (2008) Evidence for editing of human papillomavirus DNA by APOBEC3 in benign and precancerous lesions. Science 320: 230–233.
18. Conticello SG, Thomas CJ, Petersen-Mahrt SK, Neuberger MS (2005) Evolution of the AID/APOBEC family of polynucleotide (deoxy)cytidine deaminases. Mol Biol Evol 22: 367–377.
19. Jarmuz A, Chester A, Bayliss J, Gisbourne J, Dunham I, et al. (2002) An anthropoid-specific locus of orphan C to U RNA-editing enzymes on chromosome 22. Genomics 79: 285–296.
20. Malim MH (2009) APOBEC proteins and intrinsic resistance to HIV-1 infection. Philos Trans R Soc Lond B Biol Sci 364: 675–687.
21. Zhang H, Yang B, Pomerantz RJ, Zhang C, Arunachalam SC, et al. (2003) The cytidine deaminase CEM15 induces hypermutation in newly synthesized HIV-1 DNA. Nature 424: 94–98.
22. Lecossier D, Bouchonnet F, Clavel F, Hance AJ (2003) Hypermutation of HIV-1 DNA in the absence of the Vif protein. Science 300: 1112.
23. Iwatani Y, Chan DS, Wang F, Maynard KS, Sugiura W, et al. (2007) Deaminase-independent inhibition of HIV-1 reverse transcription by APOBEC3G. Nucleic Acids Res 35: 7096–7108.
24. Bishop KN, Verma M, Kim EY, Wolinsky SM, Malim MH (2008) APOBEC3G inhibits elongation of HIV-1 reverse transcripts. PLoS Pathog 4: e1000231.
25. Okeoma CM, Lovsin N, Peterlin BM, Ross SR (2007) APOBEC3 inhibits mouse mammary tumour virus replication in vivo. Nature 445: 927–930.
26. Santiago ML, Montano M, Benitez R, Messer RJ, Yonemoto W, et al. (2008) *Apobec3* encodes *Rfv3*, a gene influencing neutralizing antibody control of retrovirus infection. Science 321: 1343–1346.
27. Takeda E, Tsuji-Kawahara S, Sakamoto M, Langlois MA, Neuberger MS, et al. (2008) Mouse APOBEC3 restricts friend leukemia virus infection and pathogenesis in vivo. J Virol 82: 10998–11008.
28. Low A, Okeoma CM, Lovsin N, de las Heras M, Taylor TH, et al. (2009) Enhanced replication and pathogenesis of Moloney murine leukemia virus in mice defective in the murine APOBEC3 gene. Virology 385: 455–463.
29. Langlois MA, Kemmerich K, Rada C, Neuberger MS (2009) The AKV murine leukemia virus is restricted and hypermutated by mouse APOBEC3. J Virol 83: 11550–11559.
30. Jern P, Stoye JP, Coffin JM (2007) Role of APOBEC3 in genetic diversity among endogenous murine leukemia viruses. PLoS Genet 3: 2014–2022.
31. Chesebro B, Miyazawa M, Britt WJ (1990) Host genetic control of spontaneous and induced immunity to Friend murine retrovirus infection. Annu Rev Immunol 8: 477–499.
32. Miyazawa M, Tsuji-Kawahara S, Kanari Y (2008) Host genetic factors that control immune responses to retrovirus infections. Vaccine 26: 2981–2996.
33. Tsuji-Kawahara S, Chikaishi T, Takeda E, Kato M, Kinoshita S, et al. (2010) Persistence of viremia and production of neutralizing antibodies differentially regulated by polymorphic APOBEC3 and BAFF-R loci in Friend virus-infected mice. J Virol 84: 6082–6095.
34. Santiago ML, Benitez RL, Montano M, Hasenkrug KJ, Greene WC (2010) Innate retroviral restriction by Apobec3 promotes antibody affinity maturation in vivo. J Immunol 185: 1114–1123.
35. Miyazawa M, Nishio J, Wehrly K, Chesebro B (1992) Influence of MHC genes on spontaneous recovery from Friend retrovirus-induced leukemia. J Immunol 148: 644–647.
36. Hakata Y, Landau NR (2006) Reversed functional organization of mouse and human APOBEC3 cytidine deaminase domains. J Biol Chem 281: 36624–36631.
37. Sanville B, Dolan MA, Wollenberg K, Yan Y, Martin C, et al. (2010) Adaptive evolution of *Mus Apobec3* includes retroviral insertion and positive selection at two clusters of residues flanking the substrate groove. PLoS Pathog 6: e1000974.
38. Okeoma CM, Petersen J, Ross SR (2009) Expression of murine *APOBEC3* alleles in different mouse strains and their effect on mouse mammary tumor virus infection. J Virol 83: 3029–3038.
39. Santiago ML, Smith DS, Barrett BS, Montano M, Benitez RL, et al. (2011) Persistent Friend virus replication and disease in Apobec3-deficient mice expressing functional B-cell-activating factor receptor. J Virol 85: 189–199.
40. Mikl MC, Watt IN, Lu M, Reik W, Davies SL, et al. (2005) Mice deficient in APOBEC2 and APOBEC3. Mol Cell Biol 25: 7270–7277.
41. Hatakeyama S, Kitagawa M, Nakayama K, Shirane M, Matsumoto M, et al. (1999) Ubiquitin-dependent degradation of IκBα is mediated by a ubiquitin ligase Skp1/Cul1/F-box protein FWD1. Proc Natl Acad Sci USA 96: 3859–3863.
42. Teeter KC, Thibodeau LM, Gompert Z, Buerkle CA, Nachman MW, et al. (2010) The variable genomic architecture of isolation between hybridizing species of house mice. Evolution 64: 472–485.
43. Kozak CA, O'Neill RR (1987) Diverse wild mouse origins of xenotropic, mink cell focus-forming, and two types of ecotropic proviral genes. J Virol 61: 3082–3088.
44. Orth A, Adama T, Din W, Bonhomme F (1998) Natural hybridization between two subspecies of the house mouse, *Mus musculus domesticus* and *Mus musculus castaneus*, near Lake Casitas, California. Genome 41: 104–110.
45. Abudu A, Takaori-Kondo A, Izumi T, Shirakawa K, Kobayashi M, et al. (2006) Murine retrovirus escapes from murine APOBEC3 via two distinct novel mechanisms. Curr Biol 1615: 1565–1570.
46. Okeoma CM, Low A, Bailis W, Fan HY, Peterlin BM, et al. (2009) Induction of APOBEC3 in vivo causes increased restriction of retrovirus infection. J Virol 83: 3486–3495.
47. Mußil B, Sauermann U, Motzkus D, Stahl-Henning C, Sopper S (2011) Increased APOBEC3G and APOBEC3F expression is associated with low viral load and prolonged survival in simian immunodeficiency virus infected rhesus monkeys. Retrovirology 8: 77.
48. Biasin M, Piacentini L, Lo Caputo S, Kanari Y, Magri G, et al. (2007) Apolipoprotein B mRNA-editing enzyme, catalytic polypeptide-like 3G: a possible role in the resistance to HIV of HIV-exposed seronegative individuals. J Infect Dis 195: 960–964.
49. Boursot P, Din W, Anand R, Darviche D, Dod B, et al. (1996) Origin and radiation of the house mouse: Mitochondrial DNA phylogeny. J Evolution Biol 9: 391–415.

50. Din W, Anand R, Boursot P, Darviche D, Dod D, et al. (1996) Origin and radiation of the house mouse: Clues from nuclear genes. J Evolution Biol 9: 519–539.
51. Sawyer SL, Emerman M, Malik HS (2004) Ancient adaptive evolution of the primate antiviral DNA-editing enzyme APOBEC3G. PLoS Biol 2: E275.
52. Stocking C, Kozak C (2008) Murine endogenous retroviruses. Cell Mol Life Sci 65: 3383–3398.
53. Tomonaga K, Coffin J (1998) Structure and distribution of endogenous nonecotropic murine leukemia viruses in wild mice. J Virol 72: 8289–8300.
54. Ogawa T, Tsuji-Kawahara S, Yuasa T, Kinoshita S, Chikaishi T, et al. (2011) Natural killer cells recognize Friend retrovirus-infected erythroid progenitor cells through NKG2D-RAE-1 interactions in vivo. J Virol 85: 5423–5435.
55. Yamanaka S, Balestra ME, Ferrell LD, Fan J, Arnold KS, et al. (1995) Apolipoprotein B mRNA-editing protein induced hepatocellular carcinoma and dysplasia in transgenic animals. Proc Natl Acad Sci USA 92: 8483–8497.
56. Okazaki I, Hiai H, Kakazu N, Yamada S, Muramatsu M, et al. (2003) Constitutive expression of AID leads to tumorigenesis. J Exp Med 197: 1173–1181.
57. Kozak CA (2010) The mouse "xenotropic" gammaretroviruses and their XPR1 receptor. Retrovirology 7: 101.
58. Kidd JM, Newman TL, Tuzun E, Kaul R, Eichler EE (2007) Population stratification of a common APOBEC gene deletion polymorphism. PLoS Genet 3: e63.
59. Cascalho M (2004) Advantages and disadvantages of cytidine deamination. J Immunol 172: 6513–6518.
60. Pham P, Bransteitter R, Goodman MF (2005) Reward versus risk: DNA cytidine deaminases triggering immunity and disease. Biochemistry 44: 2703–2715.
61. Hartley JW, Rowe WP (1975) Clonal cell lines from a feral mouse embryo which lack host-range restrictions for murine leukemia viruses. Virology 65: 128–134.
62. Lander MR, Chattopadhyay SK (1984) A *Mus dunni* cell line that lacks sequences closely related to endogenous murine leukemia viruses and can be infected by ecotropic, amphotropic, xenotropic, and mink cell focus-forming viruses. J Virol 52: 695–698.
63. Chirgwin JM, Przybyla AE, MacDonald RJ, Rutter WJ (1979) Isolation of biologically active ribonucleic acid from sources enriched in ribonuclease. Biochemistry 18: 5294–5299.
64. Zuker M, Mathews DH, Turner DH (1999) Algorithms and thermodynamics for RNA secondary structure prediction: A practical guide. In: Barciszewski J, Clark BFC, eds. RNA Biochemistry and Biotechnology. Dordrecht: Kluwer Academic Publishers. pp 11–43.
65. Mathews DH, Sabina J, Zuker M, Turner DH (1999) Expanded sequence dependence of thermodynamic parameters improves prediction of RNA secondary structure. J Mol Biol 288: 911–940.
66. Veyrunes F, Dobigny G, Yang F, O'Brien PCM, Catalan J, et al. (2006) Phylogenomics of the genus *Mus* (Rodentia: Muridae): extensive genome repatterning is not restricted to the house mouse. Proc R Soc B 273: 2925–2934.
67. Lundrigan BL, Jansa SA, Tucker PK (2002) Phylogenetic relationships in the genus *Mus*, based on paternally, maternally, and biparentally inherited characters. Syst Biol 51: 410–431.
68. Guenet JL, Bonhomme F (2003) Wild mice: an ever-increasing contribution to a popular mammalian model. Trends Genet 19: 24–31.

frontiers in MICROBIOLOGY

MINI REVIEW ARTICLE
published: 21 December 2011
doi: 10.3389/fmicb.2011.00258

Structural features of antiviral APOBEC3 proteins are linked to their functional activities

Shingo Kitamura[1,2], *Hirotaka Ode*[1] *and Yasumasa Iwatani*[1,3]*

[1] Laboratory of Infectious Diseases, Department of Infectious Diseases and Immunology, Clinical Research Center, National Hospital Organization Nagoya Medical Center, Nagoya, Japan
[2] Department of Biotechnology, Graduate School of Engineering, Nagoya University, Nagoya, Japan
[3] Department of AIDS Research, Graduate School of Medicine, Nagoya University, Nagoya, Japan

Edited by:
Akio Adachi, The University of Tokushima Graduate School, Japan

Reviewed by:
Youichi Suzuki, National University of Singapore, Singapore
Kenzo Tokunaga, National Institute of Infectious Diseases, Japan

***Correspondence:**
Yasumasa Iwatani, Department of Infectious Diseases and Immunology, Clinical Research Center, National Hospital Organization Nagoya Medical Center, 4-1-1 San-no-Maru, Naka-ku, Nagoya, Japan.
e-mail: iwataniy@nnh.hosp.go.jp

Human APOBEC3 (A3) proteins are cellular cytidine deaminases that potently restrict the replication of retroviruses by hypermutating viral cDNA and/or inhibiting reverse transcription. There are seven members of this family including A3A, B, C, DE, F, G, and H, all encoded in a tandem array on human chromosome 22. A3F and A3G are the most potent inhibitors of HIV-1, but only in the absence of the virus-encoded protein, Vif. HIV-1 utilizes Vif to abrogate A3 functions in the producer cells. More specifically, Vif, serving as a substrate receptor, facilitates ubiquitination of A3 proteins by forming a Cullin5 (Cul5)-based E3 ubiquitin ligase complex, which targets A3 proteins for rapid proteasomal degradation. The specificity of A3 degradation is determined by the ability of Vif to bind to the target. Several lines of evidence have suggested that three distinct regions of A3 proteins are involved in the interaction with Vif. Here, we review the biological functions of A3 family members with special focus on A3G and base our analysis on the available structural information.

Keywords: APOBEC3, Vif, APOBEC3G, HIV, retrovirus, ubiquitin, cytidine deaminase, structure

INTRODUCTION

During coevolution of mammalian organisms and retroelements, the hosts have developed defense systems to restrict replication of these elements. The restriction factors include the A3 family of DNA cytidine deaminases, which is characterized by the presence of one or two Zn clusters consisting of (H/C)XE(X)$_{23-28}$CXXC motifs (reviewed in Wedekind et al., 2003). In humans, there are seven members of the A3 family (A3A, B, C, DE, F, G, and H), each encoded in a tandem array on chromosome 22 (Jarmuz et al., 2002; **Figure 1A**). Each protein has been found to have different inhibitory effects on various retroelements that are mediated by cytidine deamination and other mechanisms (reviewed in Goila-Gaur and Strebel, 2008; Albin and Harris, 2010). In order to overcome A3 antiviral activity, the viruses have acquired their own strategies (Yu, 2006). HIV-1 encodes the Vif protein to counteract the most potent inhibitors, human A3G (hA3G) and A3F (Sheehy et al., 2002; Wiegand et al., 2004; Zheng et al., 2004; Simon et al., 2005; Miyagi et al., 2010). Vif binds the A3 proteins and serves as a substrate receptor to recruit the Cul5-based E3 ubiquitin (Ub) ligase complex, which facilitates the polyubiquitination and subsequent proteasome-mediated degradation (Yu et al., 2003). The elimination of A3 during virus production prevents its encapsidation into progeny viruses. Thus, given Vif's critical role in eliminating A3 function, it may be viewed as one of the most attractive pharmacologic targets for an anti-HIV drug, which would restore the activity of the intrinsic antiviral factor in the context of HIV infection. Here, we briefly review what is known about A3-Vif interactions and the subsequent ubiquitination, based on the available biological and structural information.

THE HUMAN A3 FAMILY OF CYTIDINE DEAMINASES

The seven members of the human A3 family have a defining feature: each protein has one or two conserved zinc (Z)-coordinating deaminase domains. Zinc coordination is mediated by a histidine and two cysteines, which form a catalytic center for a cytidine deaminase activity. Based on the phylogenetic analysis, the Z domains fall into three types: Z1 [A3A and the C-terminal half domains (CTD) of A3B and A3G], Z2 [A3C, both halves of A3DE and A3F, and the N-terminal domains (NTD) of A3B and A3G], and Z3 (A3H; LaRue et al., 2009; **Figure 1A**). Within the Z2 types, the domain can be further subdivided into three subgroups based on the identity of the amino acid sequence: (1) the A3F NTD; (2) the A3G NTD; (3) the A3F CTD (**Figure 1B**). Each subgroup has highly conserved amino acid sequences. For example, A3F CTD is 77 and 88% identical to A3C and A3DE CTD, respectively, whereas it is 42% identical to A3G NTD. As described in more detail below, only the Z3 type (A3H) and the Z2 type (more specifically, the A3G NTD and the A3F CTD subgroups) contain a critical interface for binding HIV-1 Vif (**Figure 1B**). It is thought that there is a common structural feature for the organization of cytidine deaminases: all Z domains are believed to have a conserved core structure composed of five β-strands (β1–β5) and six α-helices (α1–α6; **Figure 2A**). Although, to date, only the three-dimensional structure of the A3G CTD has been determined by NMR (Chen et al., 2008; Furukawa et al., 2009) or by X-ray crystallography

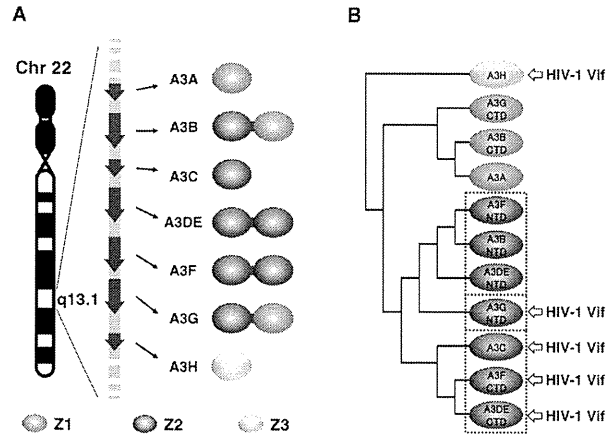

FIGURE 1 | Three types of Z domains in human A3 family. (A) Seven members of human A3 family, encoded by human chromosome 22, are illustrated. The protein products consist of one or two Z domains, each of which is phylogenetically grouped into three distinct types: Z1, Z2, and Z3. **(B)** Three subgroups of the Z2 domains are enclosed with dotted lines in the phylogenetic tree. The arrows point to the domains that are responsible for HIV-1 Vif interaction.

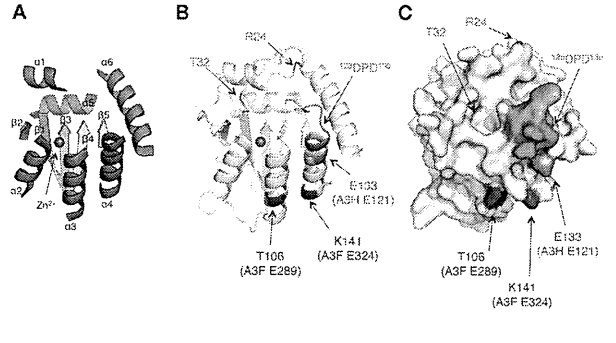

FIGURE 2 | Model structure of A3G NTD and location of responsible residues for Vif interaction. (A) Ribbon diagram of the A3 core structure for the model is depicted based on the crystal structure of the A3G CTD (PDB ID# 3IR2). The loop regions are removed. The α helices (α1–6) and β sheets (β1–5) are shown in red and yellow, respectively. **(B,C)** In the structure model, the amino acid determinants, T32, R24, and ^{128}DPD^{130}, for A3G are colored in red. The analogous residues T106 and K141 in A3F E289 and E324 (blue), and E133, corresponding to A3H E121 (green) are also shown. The critical residues, ^{125}YFW^{127}, for nucleic acid binding are colored in orange. **(C)** Predicted surface of the A3G NTD model is shown. All the critical residues are predicted to be surface exposed.

(Holden et al., 2008; Shandilya et al., 2010), no structure of the Z domain having an HIV-1 Vif interface has been solved yet.

THREE DISTINCT INTERFACES OF A3 Z DOMAINS INTERACT WITH HIV-1 VIF

The region in A3G responsible for binding to HIV-1 Vif was initially identified by comparative studies of the species specificity of A3G degradation by Vif. A single amino acid difference in hA3G, aspartic acid at position 128 (D128) versus lysine in the A3G of African green monkeys, determines species specificity by influencing Vif–A3G binding (Bogerd et al., 2004; Mangeat et al., 2004; Schrofelbauer et al., 2004; Xu et al., 2004). In addition, extensive site-direct mutagenesis revealed that the ^{128}DPD^{130} motif of A3G, located at the loop between β4 and α4 shown in red (**Figures 2B,C**), is crucial for direct binding to HIV-1 Vif (Huthoff and Malim, 2007). Furthermore, there is a report that residue T32, which may be potentially phosphorylated by protein kinase A, is also involved in the Vif–A3G interaction by collaborating with R24 (Shirakawa et al., 2008). All of these critical residues are mapped on the variable loop structure in proximity to the nucleic acid binding surface (**Figure 2B**).

In contrast, two independent studies have shown that two C-terminal A3F residues, E289 and E324, located in helices α3 and α4, respectively, are critical for the interaction with HIV-1 Vif (Albin et al., 2010; Smith and Pathak, 2010). Interestingly, in the structural model of the A3F CTD, these two residues are close to some negatively charged surface residues although the location of these residues is separate from ^{128}DPD^{130}. In accord with phylogenetic similarities, A3F E289 and E324 are highly conserved in hA3C (E106 and E141) and hA3DE CTD (E302 and E337). These findings suggest that structural features of the Vif-binding interfaces might be conserved among the A3F CTD, A3C, and A3DE CTD, but different from the A3G NTD. In the case of A3H, the interface for Vif is likely to have a surface area close to that of ^{128}DPD^{130} in the A3G NTD. The A3H gene is polymorphic, with four major haplotypes in humans. The four proteins have different levels of antiviral activity and sensitivity to HIV-1 Vif, in which haplotype II has the highest antiviral activity (Dang et al., 2008a; OhAinle et al., 2008; Harari et al., 2009; Tan et al., 2009; Li et al., 2010). By comparing the A3H variants, Zhen et al. (2010) identified a critical residue, E121, in A3H haplotype II for binding to HIV-1 (**Figures 2B,C**). Because the identity of amino acid sequences between Z2 and Z3 types, particularly the β4–α4 loop and the α4, is quite low, it is assumed that the putative Vif interface structure of A3H might be different from those of the A3G NTD or A3F CTD.

RESIDUES OF HIV-1 VIF THAT ARE CRITICAL FOR BINDING A3 PROTEINS

Extensive mutational analysis of HIV-1 Vif has led to the characterization of several distinct motifs in HIV-1 Vif that are required for formation of the Cul5-based E3 Ub ligase complex and recruitment of human A3 proteins (reviewed in Albin and Harris, 2010; **Figure 3**). The C-terminal half of Vif contains three conserved motifs: (1) the HCCH domain, which chelates zinc mediates the interaction with Cul5; (2) the SLQ motif, which binds elongin C (Elo C); and (3) the PPLP motif, which is important for Vif dimerization and recruitment of A3G, albeit by an unknown mechanism. Meanwhile, the N-terminal half of Vif is involved in the interaction with A3 proteins. **Figure 3** shows the compiled map of the critical residues that have been identified by several groups (Schrofelbauer et al., 2006; Tian et al., 2006; Russell and Pathak, 2007; He et al., 2008; Zhang et al., 2008; Chen et al., 2009; Pery et al., 2009; Zhen et al., 2010; Binka et al., 2011). Overall, it appears that the critical residues for binding to each Z domain type are discontinuous. This suggests that the interfaces in Vif might be determined by conformational constraints.

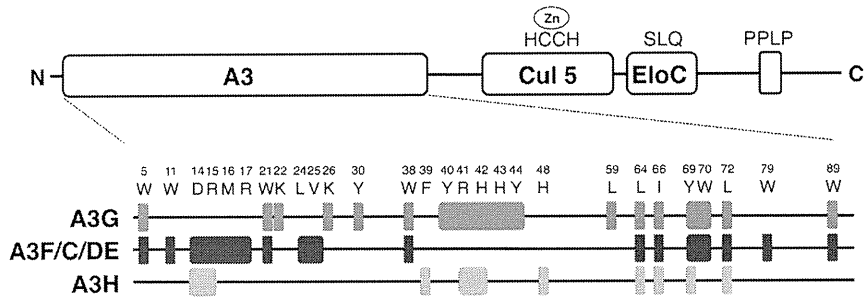

FIGURE 3 | Map of critical residues in HIV-1 Vif. Important domains in Vif (HIV-1 HXB2) are illustrated in the schematic diagram. The domains labeled "A3," "Cul5," and "Elo C" are responsible for Vif's functional interactions. The "A3" domain is responsible for binding to A3 family proteins. The amino acid sequence motifs, "HCCH," "SLQ," and "PPLP" are important for binding to Cul5, and Elo C, and Vif dimerization, respectively. The positions and the names of amino acid residues that were identified by several groups are shown. The residues that were identified as important for forming an interface with human A3 proteins are mapped in Vif, i.e., A3G (red), A3F, A3C, and A3DE (blue), and A3H (green).

Interestingly, some residues are unique among the three types of Z domains, suggesting that such residues might determine binding specificity. For example, K22, K26, Y30, Y40, H43, Y44, and L59 are important for interaction only with A3G, whereas the residues W11, M16, R17, L24, V25, and W79 are required for specific interactions with A3F. These residues tend to have two characteristics: they are positively charged or hydrophobic. Interestingly, the electrostatic charge of the Vif residues is mostly positive whereas the key residues that comprise the A3 interfaces are negatively charged. Thus, such electrostatic interactions might be one of the common features for binding between human A3 proteins and HIV-1 Vif. This could also determine the species-specific interactions between Vif and A3 proteins, as demonstrated in the case of Vif–A3G (Bogerd et al., 2004; Mangeat et al., 2004; Schrofelbauer et al., 2004; Xu et al., 2004). In contrast to the aforementioned regions, there are some aromatic or hydrophobic residues, W5, W21, W38, W70, and W89, which are commonly responsible for binding to two (the A3G NTD and the A3F CTD), or L64, I66, Y69, and L72 to all types of Z domains. These regions could play fundamental roles in maintaining the overall conformation of A3-binding interfaces or could form a partly shared structure of the interface for either two or all Z domains.

VIF-MEDIATED UBIQUITINATION/DEGRADATION

Information concerning the specific interaction between Vif and A3G in the E3 Ub ligase complex suggests that there may be a specific mechanism for Ub conjugation of the A3G protein. Previously, our studies using structure-guided mutagenesis demonstrated that four lysine residues (K297, 301, 303, and 334) near the C-terminal end of A3G are critical sites for HIV-1 Vif-mediated A3G ubiquitination and degradation (Iwatani et al., 2009). The data suggested that these sites, which are located on the opposite end of A3G relative to the Vif-binding interface, might be specifically dictated by the rigid structure of the Cul5-based scaffold. In addition, the study clearly demonstrated that the additional residues, particularly lysines near the C-terminal tag of A3G could be potential targets for Vif-induced ubiquitination. However, recently, Wang et al. (2011) showed that a detectable level of Vif-mediated ubiquitination occurs at the N-terminus in addition to certain lysine residues within 20 lysine residues of A3G. In contrast, another group could detect no N-terminal ubiquitination (Dang et al., 2008b). Although these apparent contradictions might be due to differences in the detection level of ubiquitination, it is important to consider the possibility that different tags attached at the C-terminal end of an A3G protein could create potential ubiquitination sites and/or mask the area where the four lysine residues are located (Iwatani et al., 2009). Moreover, while ubiquitination is associated primarily with the lysines in the CTD, the observation that there is also N-terminal ubiquitination could be of interest. The evidences of two distal ubiquitination sites in A3G may provide important structural insight, which implies two distinct types of structural configuration for Vif–A3G interaction. Further studies are needed to clarify Vif-mediated ubiquitination in the context of the E3 Ub ligase complex and to allow us to answer the following two questions: (1) How can we rationalize the relationship between the configuration of the N-terminal end and the proximal Vif-binding interface? (2) In particular, how can the Ub molecules be conjugated at the N-terminus, which is predicted to be a structurally flexible end?

CONCLUSION

Phylogenetic analyses and genetic studies of A3 and Vif have provided important evidence for three distinct types of interactions between human A3 and HIV-1 Vif proteins, which are determined by the characteristic Z domain types of A3G, A3F/C/DE, and A3H. Further understanding of Vif–A3 interactions could advance efforts to develop novel anti-HIV drugs, which would function as anti-Vif inhibitors. Although presenting a tremendous challenge, complementary studies focusing on the structure of the Vif-interactive A3 domain and Vif are also critical to accelerate future progress in this field.

ACKNOWLEDGMENTS

We thank Dr. Judith G. Levin (NIH, NICHD) for helpful discussions. This work was supported in part by a grant-in-aid for Scientific Research from the Ministry of Education, Culture, Sports, Science and Technology of Japan and by a grant for HIV/AIDS research from the Ministry of Health, Labor, and Welfare of Japan.

REFERENCES

Albin, J. S., and Harris, R. S. (2010). Interactions of host APOBEC3 restriction factors with HIV-1 in vivo: implications for therapeutics. *Expert Rev. Mol. Med.* 12, e4.

Albin, J. S., LaRue, R. S., Weaver, J. A., Brown, W. L., Shindo, K., Harjes, E., Matsuo, H., and Harris, R. S. (2010). A single amino acid in human APOBEC3F alters susceptibility to HIV-1 Vif. *J. Biol. Chem.* 285, 40785–40792.

Binka, M., Ooms, M., Steward, M., and Simon, V. (2011). The activity spectrum of Vif from multiple HIV-1 subtypes against APOBEC3G, APOBEC3F and APOBEC3H. *J. Virol.* (in press).

Bogerd, H. P., Doehle, B. P., Wiegand, H. L., and Cullen, B. R. (2004). A single amino acid difference in the host APOBEC3G protein controls the primate species specificity of HIV type 1 virion infectivity factor. *Proc. Natl. Acad. Sci. U.S.A.* 101, 3770–3774.

Chen, G., He, Z., Wang, T., Xu, R., and Yu, X. F. (2009). A patch of positively charged amino acids surrounding the human immunodeficiency virus type 1 Vif SLVx4Yx9Y motif influences its interaction with APOBEC3G. *J. Virol.* 83, 8674–8682.

Chen, K. M., Harjes, E., Gross, P. J., Fahmy, A., Lu, Y., Shindo, K., Harris, R. S., and Matsuo, H. (2008). Structure of the DNA deaminase domain of the HIV-1 restriction factor APOBEC3G. *Nature* 452, 116–119.

Dang, Y., Siew, L. M., Wang, X., Han, Y., Lampen, R., and Zheng, Y. H. (2008a). Human cytidine deaminase APOBEC3H restricts HIV-1 replication. *J. Biol. Chem.* 283, 11606–11614.

Dang, Y., Siew, L. M., and Zheng, Y. H. (2008b) APOBEC3G is degraded by the proteasomal pathway in a Vif-dependent manner without being polyubiquitylated. *J. Biol. Chem.* 283, 13124–13131.

Furukawa, A., Nagata, T., Matsugami, A., Habu, Y., Sugiyama, R., Hayashi, F., Kobayashi, N., Yokoyama, S., Takaku, H., and Katahira, M. (2009). Structure, interaction and real-time monitoring of the enzymatic reaction of wild-type APOBEC3G. *EMBO J.* 28, 440–451.

Goila-Gaur, R., and Strebel, K. (2008). HIV-1 Vif, APOBEC, and intrinsic immunity. *Retrovirology* 5, 51.

Harari, A., Ooms, M., Mulder, L. C., and Simon, V. (2009). Polymorphisms and splice variants influence the antiretroviral activity of human APOBEC3H. *J. Virol.* 83, 295–303.

He, Z., Zhang, W., Chen, G., Xu, R., and Yu, X. F. (2008). Characterization of conserved motifs in HIV-1 Vif required for APOBEC3G and APOBEC3F interaction. *J. Mol. Biol.* 381, 1000–1011.

Holden, L. G., Prochnow, C., Chang, Y. P., Bransteitter, R., Chelico, L., Sen, U., Stevens, R. C., Goodman, M. F., and Chen, X. S. (2008). Crystal structure of the anti-viral APOBEC3G catalytic domain and functional implications. *Nature* 456, 121–124.

Huthoff, H., and Malim, M. H. (2007). Identification of amino acid residues in APOBEC3G required for regulation by human immunodeficiency virus type 1 Vif and Virion encapsidation. *J. Virol.* 81, 3807–3815.

Iwatani, Y., Chan, D. S., Liu, L., Yoshii, H., Shibata, J., Yamamoto, N., Levin, J. G., Gronenborn, A. M., and Sugiura, W. (2009). HIV-1 Vif-mediated ubiquitination/degradation of APOBEC3G involves four critical lysine residues in its C-terminal domain. *Proc. Natl. Acad. Sci. U.S.A.* 106, 19539–19544.

Jarmuz, A., Chester, A., Bayliss, J., Gisbourne, J., Dunham, I., Scott, J., and Navaratnam, N. (2002). An anthropoid-specific locus of orphan C to U RNA-editing enzymes on chromosome 22. *Genomics* 79, 285–296.

LaRue, R. S., Andresdottir, V., Blanchard, Y., Conticello, S. G., Derse, D., Emerman, M., Greene, W. C., Jonsson, S. R., Landau, N. R., Lochelt, M., Malik, H. S., Malim, M. H., Munk, C., O'Brien, S. J., Pathak, V. K., Strebel, K., Wain-Hobson, S., Yu, X. F., Yuhki, N., and Harris, R. S. (2009). Guidelines for naming nonprimate APOBEC3 genes and proteins. *J. Virol.* 83, 494–497.

Li, M. M., Wu, L. I., and Emerman, M. (2010). The range of human APOBEC3H sensitivity to lentiviral Vif proteins. *J. Virol.* 84, 88–95.

Mangeat, B., Turelli, P., Liao, S., and Trono, D. (2004). A single amino acid determinant governs the species-specific sensitivity of APOBEC3G to Vif action. *J. Biol. Chem.* 279, 14481–14483.

Miyagi, E., Brown, C. R., Opi, S., Khan, M., Goila-Gaur, R., Kao, S., Walker, R. C. Jr., Hirsch, V., and Strebel, K. (2010). Stably expressed APOBEC3F has negligible antiviral activity. *J. Virol.* 84, 11067–11075.

OhAinle, M., Kerns, J. A., Li, M. M., Malik, H. S., and Emerman, M. (2008). Antiretroelement activity of APOBEC3H was lost twice in recent human evolution. *Cell Host Microbe* 4, 249–259.

Pery, E., Rajendran, K. S., Brazier, A. J., and Gabuzda, D. (2009). Regulation of APOBEC3 proteins by a novel YXXL motif in human immunodeficiency virus type 1 Vif and simian immunodeficiency virus SIVagm Vif. *J. Virol.* 83, 2374–2381.

Russell, R. A., and Pathak, V. K. (2007). Identification of two distinct human immunodeficiency virus type 1 Vif determinants critical for interactions with human APOBEC3G and APOBEC3F. *J. Virol.* 81, 8201–8210.

Schrofelbauer, B., Chen, D., and Landau, N. R. (2004). A single amino acid of APOBEC3G controls its species-specific interaction with virion infectivity factor (Vif). *Proc. Natl. Acad. Sci. U.S.A.* 101, 3927–3932.

Schrofelbauer, B., Senger, T., Manning, G., and Landau, N. R. (2006). Mutational alteration of human immunodeficiency virus type 1 Vif allows for functional interaction with nonhuman primate APOBEC3G. *J. Virol.* 80, 5984–5991.

Shandilya, S. M., Nalam, M. N., Nalivaika, E. A., Gross, P. J., Valesano, J. C., Shindo, K., Li, M., Munson, M., Royer, W. E., Harjes, E., Kono, T., Matsuo, H., Harris, R. S., Somasundaran, M., and Schiffer, C. A. (2010). Crystal structure of the APOBEC3G catalytic domain reveals potential oligomerization interfaces. *Structure* 18, 28–38.

Sheehy, A. M., Gaddis, N. C., Choi, J. D., and Malim, M. H. (2002). Isolation of a human gene that inhibits HIV-1 infection and is suppressed by the viral Vif protein. *Nature* 418, 646–650.

Shirakawa, K., Takaori-Kondo, A., Yokoyama, M., Izumi, T., Matsui, M., Io, K., Sato, T., Sato, H., and Uchiyama, T. (2008). Phosphorylation of APOBEC3G by protein kinase A regulates its interaction with HIV-1 Vif. *Nat. Struct. Mol. Biol.* 15, 1184–1191.

Simon, V., Zennou, V., Murray, D., Huang, Y., Ho, D. D., and Bieniasz, P. D. (2005). Natural variation in Vif: differential impact on APOBEC3G/3F and a potential role in HIV-1 diversification. *PLoS Pathog.* 1, e6. doi:10.1371/journal.ppat.0010006

Smith, J. L., and Pathak, V. K. (2010). Identification of specific determinants of human APOBEC3F, APOBEC3C, and APOBEC3DE and African green monkey APOBEC3F that interact with HIV-1 Vif. *J. Virol.* 84, 12599–12608.

Tan, L., Sarkis, P. T., Wang, T., Tian, C., and Yu, X. F. (2009). Sole copy of Z2-type human cytidine deaminase APOBEC3H has inhibitory activity against retrotransposons and HIV-1. *FASEB J.* 23, 279–287.

Tian, C., Yu, X., Zhang, W., Wang, T., Xu, R., and Yu, X. F. (2006). Differential requirement for conserved tryptophans in human immunodeficiency virus type 1 Vif for the selective suppression of APOBEC3G and APOBEC3F. *J. Virol.* 80, 3112–3115.

Wang, Y., Shao, Q., Yu, X., Kong, W., Hildreth, J. E., and Liu, B. (2011). N-terminal hemagglutinin tag renders lysine-deficient APOBEC3G resistant to HIV-1 Vif-induced degradation by reduced polyubiquitination. *J. Virol.* 85, 4510–4519.

Wedekind, J. E., Dance, G. S., Sowden, M. P., and Smith, H. C. (2003). Messenger RNA editing in mammals: new members of the APOBEC family seeking roles in the family business. *Trends Genet.* 19, 207–216.

Wiegand, H. L., Doehle, B. P., Bogerd, H. P., and Cullen, B. R. (2004). A second human antiretroviral factor, APOBEC3F, is suppressed by the HIV-1 and HIV-2 Vif proteins. *EMBO J.* 23, 2451–2458.

Xu, H., Svarovskaia, E. S., Barr, R., Zhang, Y., Khan, M. A., Strebel, K., and Pathak, V. K. (2004). A single amino acid substitution in human APOBEC3G antiretroviral enzyme confers resistance to HIV-1 virion infectivity factor-induced depletion. *Proc. Natl. Acad. Sci. U.S.A.* 101, 5652–5657.

Yu, X., Yu, Y., Liu, B., Luo, K., Kong, W., Mao, P., and Yu, X. F. (2003). Induction of APOBEC3G ubiquitination and degradation by an HIV-1 Vif-Cul5-SCF complex. *Science* 302, 1056–1060.

Yu, X. F. (2006). Innate cellular defenses of APOBEC3 cytidine deaminases and viral counter-defenses. *Curr. Opin. HIV AIDS* 1, 187–193.

Zhang, W., Chen, G., Niewiadomska, A. M., Xu, R., and Yu, X. F. (2008). Distinct determinants in HIV-1 Vif and human APOBEC3 proteins are required for the suppression of diverse host anti-viral proteins. *PLoS ONE* 3, e3963. doi:10.1371/journal.pone.0003963

Zhen, A., Wang, T., Zhao, K., Xiong, Y., and Yu, X. F. (2010). A single amino acid difference in human APOBEC3H variants determines HIV-1 Vif sensitivity. *J. Virol.* 84, 1902–1911.

Zheng, Y. H., Irwin, D., Kurosu, T., Tokunaga, K., Sata, T., and Peterlin, B. M. (2004). Human APOBEC3F is another host

factor that blocks human immunodeficiency virus type 1 replication. *J. Virol.* 78, 6073–6076.

Conflict of Interest Statement: The authors declare that the research was conducted in the absence of any commercial or financial relationships that could be construed as a potential conflict of interest.

Received: 14 November 2011; accepted: 02 December 2011; published online: 21 December 2011.
Citation: Kitamura S, Ode H and Iwatani Y (2011) Structural features of antiviral APOBEC3 proteins are linked to their functional activities. Front. Microbio. 2:258. doi: 10.3389/fmicb.2011.00258
This article was submitted to Frontiers in Virology, a specialty of Frontiers in Microbiology.